A collection of genetic mouse lines and related tools for inducible and reversible intersectional misexpression

Elham Ahmadzadeh[1], N. Sumru Bayin[2], Xinli Qu[1], Aditi Singh[1], Linda Madisen[3], Daniel Stephen[2], Hongkui Zeng[3], Alexandra L. Joyner[2]* and Alberto Rosello-Diez[1]*

[1] *Australian Regenerative Medicine Institute, Monash University. Clayton, VIC 3800. Australia.*

[2] *Developmental Biology Program. Sloan Kettering Institute. New York, NY 10065. USA.*

[3] *Allen Institute for Brain Science. Seattle, WA 98109. USA*

***Correspondence:** alberto.rosellodiez@monash.edu; joynera@mskcc.org

Summary statement

Ahmadzadeh et al. present a collection of four mouse lines and genetic tools for misexpression-mediated manipulation of cellular activity with high spatiotemporal control, in a reversible manner.

Abstract

Thanks to many advances in genetic manipulation, mouse models have become very powerful in their ability to interrogate biological processes. In order to precisely target expression of a gene of interest to particular cell types, intersectional genetic approaches utilizing two promoter/enhancers unique to a cell type are ideal. Within these methodologies, variants that add temporal control of gene expression are the most powerful. We describe the development, validation and application of an intersectional approach that involves three transgenes, requiring the intersection of two promoter/enhancers to target gene expression to precise cell types. Furthermore, the approach utilizes available lines expressing tTA/rTA to control timing of gene expression based on whether doxycycline is absent or present, respectively. We also show that the approach can be extended to other animal models, using chicken embryos. We generated three mouse lines targeted at the *Tigre* (*Igs7*) locus with TRE-loxP-tdTomato-loxP upstream of three genes (*p21*, *DTA* and *Ctgf*) and combined them with Cre and tTA/rtTA lines that target expression to the cerebellum and limbs. Our tools will facilitate unraveling biological questions in multiple fields and organisms.

Keywords

Cre, tTA, rtTA, intersectional genetics, inducible and reversible gene misexpression, tissue-specific, Tigre locus, DRAGON allele, p21, Ccn2/Ctgf, diphtheria toxin, DTA, tox176.

33 **INTRODUCTION**

34

35 The wealth of genetic tools that have been developed for mouse to study biological questions *in*
36 *vivo* have enabled extremely sophisticated experiments to be conducted. Especially useful are tools
37 that have a modular nature. One approach for inducing gene mis-expression is to combine a mouse
38 line carrying a driver module that expresses a protein (transcription factor) that induces gene
39 expression only when the right genetic elements (DNA binding sites) are present with a line
40 carrying an effector module that contains the necessary genetic elements upstream of a gene of
41 interest (GOI). In this way only the offspring combining both modules will specifically express the
42 GOI in particular cells defined by the driver module (Kaczmarczyk and Jackson, 2015; Rosen et al.,
43 2015). This system can be modified to implement temporal and spatial control of gene expression
44 by making it dependent on the activity of site specific recombinases (SSRs) (e.g. Cre), and by
45 expressing SSRs from gene promoters or loci with specific expression patterns (Smedley et al.,
46 2011). One drawback of using SSR systems, including inducible versions that allow for temporal
47 control (e.g. CreER) (Brocard et al., 1998; Feil et al., 1997; Feil et al., 2009; Metzger et al., 1995),
48 is that recombination of the target sites (loxP in the case of Cre) is irreversible. Hence, if
49 misexpression of a GOI is dependent only on Cre activity, it cannot be reversed, and therefore
50 studying any recovery process after a transient genetic manipulation is not possible.
51 The possibility of reversibility has been resolved by using other driver-effector combinations, the
52 most prevalent in mouse being the Tet system, based on the tetracycline (Tet) resistance operon of
53 *E. coli* (Hillen and Berens, 1994). In the first version of this system, a transactivator fusion protein
54 composed of the tetracycline repressor (tetR) and the activating domain of the herpes simplex viral
55 protein 16 (VP16) regulate the expression of a GOI by placing a Tet-responsive element (TRE)
56 containing tet-operator sequences (tetO) upstream of the gene sequence. This system is known as
57 Tet-Off, because in the presence of tetracycline or its analog doxycycline (Dox), the affinity of tetR
58 to *tetO* sequences diminishes by 9 orders of magnitude, so that expression of the gene of interest is
59 greatly reduced (Gossen and Bujard, 1992; St-Onge et al., 1996). Conversely, the Tet-On system is
60 based on a reverse tetracycline-controlled transactivator (*rtTA*) derived from tTA through four
61 amino acid changes in the tetR DNA binding moiety. This alters the binding properties of rtTA such
62 that it can only recognize the *tetO* sequences in the presence of Dox (Gossen et al., 1995; Urlinger
63 et al., 2000). A problem that for many years encumbered systems using tTA and rtTA (referred to
64 as (r)tTA) was that the TRE DNA sequences can be inactivated through epigenetic mechanisms,
65 rendering them unreliable unless de-repressed by additional genetic modules (Godecke et al., 2017).
66 This drawback was overcome when a systematic screen identified a locus in the mouse genome that
67 does not show this inactivation (Zeng et al., 2008). Indeed, *Tigre* (aka *Igs7*) is an intergenic region

68 on mouse chromosome 9 that provides a safe harbor from which TRE-dependent expression can be
69 tightly regulated (hence the name).
70 Despite these advances, all systems are limited by the fact that individual promoters/enhancers or
71 gene loci often drive the expression of Cre/(r)tTA in a broader area (or more cell types) than what is
72 required for the experiment, leading to insufficient specificity. Several intersectional approaches
73 have been developed that allow for greater control over what cells are genetically manipulated. In
74 one approach separate fragments of the Cre recombinase (known as "split cre") are expressed from
75 distinct drivers (promoter/enhancer sequences), resulting in Cre activity (loxP excision) only in the
76 intersectional cell population where both halves of Cre are expressed (Hirrlinger et al., 2009).
77 Another intersectional approach utilizes responder modules that depend on two types of
78 recombinases (e.g. Cre and Flp), such as the systems developed by the Dymecki lab (Dymecki and
79 Kim, 2007). However, neither approach allows for the GOI expression to be regulated in a
80 reversible manner.
81 One strategy that allows for both precision of cell-type targeting and reversibility of gene mis-
82 expression was recently developed by our labs (Madisen et al., 2015; Rosello-Diez et al., 2018).
83 The approach involves combining the Cre/loxP and Tet systems such that the *Tigre* locus contains a
84 double conditional allele in which expression of the GOI depends both on previous exposure to Cre
85 (to prime the system through elimination of a floxed STOP sequence upstream of the GOI) and on
86 the activity of (r)tTA (through a TRE sequence upstream of the loxP-STOP-loxP-GOI-polyA
87 cassette). The version of this system that includes a tdTomato (tdT) coding sequence for the floxed-
88 STOP cassette was called DRAGON (Fig. 1A), standing for Doxycycline-dependent and
89 Recombinase-Activated Gene OverexpressioN (Rosello-Diez et al., 2018). The GOI in the first
90 DRAGON line was the cell-cycle suppressor gene *p21* ($Tigre^{Dragon\text{-}p21}$) and it was used to study
91 cellular compensation mechanisms in the developing limb bones upon cell cycle blockade (Rosello-
92 Diez et al., 2018). Since the DRAGON approach relies on two promoter/enhancers, it is
93 intersectional (Fig. 1B), enabling the study of specific tissue-type dependent effects of gene
94 misexpression. In addition, due to its dependence on (r)tTA, the system is inducible and reversible
95 (Fig. 1C, D), allowing the effect of different times and durations of misexpression to be tested.
96 Finally, by developing additional modules with particular GOIs involved in a specific cellular
97 process (e.g. to reduce cell numbers by either blocking proliferation or inducing cell death), the
98 system can effectively determine how different types of insults influence a biological process.
99 Here we describe a series of new $Tigre^{Dragon}$ lines (Fig. 1E) and provide a proof-of-principle for the
100 kind of uses that they enable in two developing organs, the cartilage that drives long-bone growth in
101 the limb (Kronenberg, 2003) and the excitatory cells of the cerebellar nuclei required for cerebellum
102 growth (Willett et al., 2019). We also describe non-intersectional applications for comparison

103 purposes, and the possibility of using these tools for transient gene misexpression in avian models.
104
105 **RESULTS**
106 **A *Tigre*$^{Dragon\text{-}DTA}$ model can be used to generate acute tissue-specific cell ablation.**
107 A common theme in developmental and regenerative biology is that different responses are elicited
108 by cell ablation compared to defective cell proliferation. Therefore, to complement our *Tigre*$^{Dragon\text{-}p21}$
109 line, we generated an intersectional *Tigre*$^{Dragon\text{-}DTA}$ model (see Methods, Fig. 2A and (Willett et
110 al., 2019)) to enable cell ablation with tissue specificity and temporal control, via expression of
111 attenuated diphtheria toxin fragment A (Breitman et al., 1990). To kill some of the excitatory
112 cerebellar nuclei neurons (eCN) that are the main output neurons of the cerebellum, we combined it
113 with two transgenes: *Atoh1-tTA* (Tet-Off) (Willett et al., 2019) and *Atoh1-Cre* (Matei et al., 2005).
114 Both transgenes are expressed in cells after they leave the progenitor zone called the rhombic lip.
115 Since both the eCN and the precursors of another excitatory cell type, the cerebellar granule cells,
116 express *Atoh1* but at different time points (E9-12 and after E13, respectively (Machold and Fishell,
117 2005)), the mice were provided with Doxycycline (Dox) starting at embryonic day 13.5 (E13.5) to
118 shut down tTA activity after the eCN had extinguished *Atoh1* expression, thus restricting DTA
119 expression to the eCN and sparing the granule cell precursors (Fig 2B). As shown in Fig. 2C-F,
120 whereas control cerebella showed almost no cell death, in the cerebellum of the *Atoh1-tTA/+;*
121 *Atoh1-Cre*/+; *Tigre*$^{Dragon\text{-}DTA/+}$ mice given Dox at E13.5 onwards (*AC-eCN-DTA* model, AC
122 designates *Atoh1-Cre* and eCN designates eCN-expression using *Atoh1-tTA*) ectopic cell death
123 (marked by TUNEL staining) was detected specifically in the Nuclear Transitory Zone (NTZ), the
124 region where the precursors of the eCN first migrate to after leaving the rhombic lip. tdTom^{+} cells
125 were detected in the cells expected to express *Atoh1-tTA* including the NTZ, granule cell precursors
126 in the external granule cell layer (EGL) and in *Atoh1*-derived precerebellar hindbrain nuclei (Fig.
127 2E). Quantification of cell death revealed an 8.85±3.35 fold increase in TUNEL^{+} particles in the
128 NTZ in *AC-eCN-DTA* animals compared to their control littermates (*Tigre*$^{Dragon\text{-}DTA/+}$) at E13.5 (n=3
129 per condition, Fig. 2G). At P1, the number of eCN, revealed by MEIS2 nuclear immunostaining,
130 was reduced by more than 50% in *AC-eCN-DTA* cerebella as compared to controls (Fig. 2H-J).
131 One complication of using *Atoh1*-driven transgenes to target cells in the cerebellum is that they are
132 also expressed in many precerebellar neurons in nuclei of the hindbrain at E10-13, as well as
133 ectopic expression elsewhere in the brain and expression in other organs. Therefore, we used an
134 intersectional approach to limit the expression of DTA to cells in the cerebellum and only a few
135 nuclei in the isthmus in the midbrain-hindbrain junction (Machold and Fishell, 2005) by
136 incorporating our *En1*^{Cre} knock-in line (Kimmel et al., 2000). This line expresses Cre in the
137 midbrain and rhombomere 1 of the hindbrain starting at E8 and thus includes the rhombic lip (Fig.

138 3A). By using *Atoh1-tTA/+; En1-Cre; Tigre*$^{Dragon\text{-}DTA/+}$ mice and providing Dox starting at E13.5 to
139 shut down tTA activity in granule cell precursors (see Fig. 2B), we restricted DTA expression
140 primarily to the eCN (Fig. 3B-E, *EC-eCN-DTA* model, EC designates *En1*^{Cre}). Analysis of E13.5
141 embryos before Dox was administered showed ectopic cell death specifically in the region of the
142 rhombic lip where cells first turn on the *Atoh1-tTA* transgene in *EC-eCN-DTA* mice (marked by
143 TUNEL staining, Fig. 3B-E). Since *En1*^{Cre} turns on earlier than *Atoh1-Cre* in the eCN precursors,
144 cell death was observed in the rhombic lip rather than in the NTZ (where it was seen in *AC-eCN-*
145 *DTA* embryos). Quantification of cell death revealed a 14.20 ± 2.43 fold increase in TUNEL^{+}
146 particles in the rhombic lip region of the *EC-eCN-DTA* embryos compared to controls (*Tigre*$^{Dragon\text{-}}$
147 $^{DTA/+}$ or *Atoh1-tTA/+; Tigre*$^{Dragon\text{-}DTA/+}$, n=3/condition, Fig. 3F). Furthermore, unlike in *AC-eCN-*
148 *DTA* embryos, no tdTom^{+} cells were detected in the NTZ, consistent with the majority of eCN
149 being ablated before tdTom is induced since Cre is present before the *Atoh1-tTA* transgene is
150 expressed (Fig. 3E). In addition, at E13.5 we observed tdTom^{+} cells in the hindbrain posterior to
151 rhombomere 1 that belong to the Atoh1-lineage and do not express *En1* or Cre (Machold and
152 Fishell, 2005) (Fig. 3D,E). At P30, the number of eCN, revealed by counting of the large NeuN^{+}
153 neurons in the cerebellar nuclei was reduced by ~60% in *EC-eCN-DTA* cerebella as compared to
154 the controls (Fig. 3G). As a consequence of the embryonic killing of the eCN, the size of the
155 cerebellum was reduced by approximately one half (Fig. 3H-J). The decrease in cerebellum size at
156 P30, and thus growth during development, was greater with the intersectional *EC-eCN-DTA* model
157 than with the *AC-eCN-DTA* model (Willett et al. 2019), likely because in the latter some eCN do
158 not express DTA because *Atoh1-Cre* is only transiently expressed in eCN precursors and once it is
159 expressed it must first delete the floxed *tdTom* gene in the *Tigre*$^{Dragon\text{-}DTA}$ allele to allow DTA to be
160 expressed and kill cells. Consistent with this, in *AC-eCN-DTA* E13.5 embryos tdTom^{+} cells were
161 detected in the NTZ and granule cell precursors (Fig. 2). Comparison of the intersectional approach
162 (*Atoh1-tTA* and *En1*^{Cre}) with the double *Atoh1*-driven transgenes (*Atoh1-tTA* and *Atoh1-Cre*)
163 demonstrates the unique utility of each approach, with the *En1* and *Atoh1* intersectional approach
164 achieving more precise cell targeting of DTA, and also earlier and therefore more widespread
165 killing of eCN. Furthermore, analysis of *Tigre*$^{Dragon\text{-}DTA/+}$ and *Atoh1-tTA/+; Tigre*$^{Dragon\text{-}DTA/+}$ mice
166 demonstrates that the transgene does not have leaky expression of DTA when the *tdTom* STOP
167 sequence is present, while analysis of either of the control transgenic embryos with *Cre* alone
168 (*Atoh1-Cre* or *En1*^{Cre}) demonstrates lack of leaky expression of the recombined allele in the
169 absence of tTA (Fig 2. C-E and Fig. 3 B-D).
170 To further demonstrate the utility of the *Tigre*$^{Dragon\text{-}DTA}$ line we bred it with mice bearing a left-
171 lateral plate mesoderm specific *Pitx2-Cr*e (Shiratori et al., 2006) and either one of two possible
172 cartilage-specific (r)tTAs: *Col2a1-tTA* (Rosello-Diez et al., 2018) (for E15.5 experiment, no Dox

173 added) or *Col2a1-rtTA* (Posey et al., 2009) (for P1 experiment, Dox added at E12.5) to achieve
174 unilateral ablation in the cartilage of the left limbs (*PC-Cart-DTA* model, PC designates *Pitx2-Cr*e
175 and Cart designates cartilage-specific expression using *Col2a1-(r)tTA;* Fig. 4A). At E15.5 (i.e. ~3
176 days after activation), TUNEL staining revealed increased cell death in the left cartilage compared
177 to the right one (Fig. 4B), which was also seen at P1 (Fig. 4D). Quite strikingly, maintenance of the
178 injury until P0 led to the generation of acellular gaps in the left cartilage (dashed lines, Fig. 4C,
179 n=3). This injury led to a significant left-right limb asymmetry at P0, with the left bones 10-15%
180 shorter than the contralateral ones (Fig. 4E).
181 With toxins as powerful as DTA, it is important to target only the population of interest, which is
182 one of the main advantages of our intersectional system. Indeed, *Pitx2-Cre* is expressed not only in
183 the left lateral plate mesenchyme, but also in some regions of the heart (Shiratori et al., 2006),
184 which can lead to unwanted effects. For example, if expression of diphtheria toxin receptor is
185 activated by *Pitx2-Cre,* injection of diphtheria toxin leads to cell death not only in the left limb
186 mesenchyme, but also in the heart, affecting survival of the experimental animals (Supplementary
187 Fig. 1A and (Rosello-Diez et al., 2017)). Importantly, with our intersectional system almost no cell
188 death was detected in the hearts of *PC-DTA* controls or Dox-treated *PC-Cart-DTA* embryos
189 (Supplementary Fig. 1B-D), confirming the validity of the intersectional approach and lack of DTA
190 expression in the absence of active (r)tTA. In summary, combining our $Tigre^{Dragon\text{-}DTA}$ line with
191 different pairs of the available *Cre* and *(r)tTA* lines provides a valuable resource to selectively
192 ablate cells with high spatiotemporal precision.
193
194 **Unilateral misexpression of Connective Tissue Growth Factor in the growing skeletal**
195 **elements leads to bone asymmetry.**
196 We next searched for a GOI that could provide a versatile tool for transiently manipulating a variety
197 of biological processes, such as development, homeostasis and repair. We reasoned that a molecule
198 capable of interacting with several of the most common signaling pathways would be an ideal
199 candidate. Connective tissue growth factor (CTGF) has been described to exert such a pleiotropic
200 effect (Takigawa, 2013). Indeed, CTGF can interact with several signaling receptors, is considered
201 as a hub in a network of molecular interactions, and plays a role in the harmonization of cartilage
202 and bone development (Kubota and Takigawa, 2015), cardiovascular function (Ponticos, 2013),
203 fibrosis, tendon healing (Tarafder et al., 2017), etc. We thus generated a $Tigre^{Dragon\text{-}Ctgf}$ mouse
204 model (see Methods) and combined it with mice bearing left-lateral plate mesoderm specific *Pitx2-*
205 *Cre* (Shiratori et al., 2006) and a cartilage-specific *Col2a1-tTA* (Tet-Off) (Rosello-Diez et al., 2018)
206 to achieve unilateral expression of CTGF in the cartilage of the left limbs (*PC-Cart-Ctgf* model,
207 Fig. 5A). By P0-P1, whereas the expression of *Ctgf* in the distal cartilage of the right *PC-Cart-Ctgf*

208 radius was very similar to the expression in WT animals (Fig. 5B-C), the expression in the left *PC-*
209 *Cart-Ctgf* element was more widespread (Fig. 5C). Interestingly, the ectopic expression of CTGF
210 led to reduced growth of the left bones as early as embryonic day (E) 17.5, including deformation of
211 the radius and ulna at or after postnatal day (P) 5 (Fig. 5D). While mechanistic studies will be
212 reported elsewhere, we are currently investigating whether this phenotype is related to increased
213 vascular invasion and altered osteoclast activity, similar to that reported upon increased VEGF
214 activity (Maes et al., 2010). Given its strong effects in a plethora of tissues and processes, we expect
215 the *Tigre*$^{Dragon\text{-}Ctgf}$ mouse line to become a valuable tool for life scientists working on diverse topics.
216
217 **A model for reversible connective tissue growth factor misexpression in the growing skeletal**
218 **elements reveals different outcomes of transient vs. permanent expression.**
219 Besides its intersectional quality, a key aspect of the *Dragon* system is its reversibility. As a second
220 proof-of-principle for testing this application, we repeated the *PC-Cart-Ctgf* experiment and
221 supplied Dox to shut down tTA expression at E17.5 (Fig. 6A), soon after the phenotype is obvious
222 (Fig. 5D). As expected, *Ctgf* ceased to be overexpressed in the cartilage by P0-P1 (Fig. 6B).
223 Moreover, when the extent of asymmetry was compared between continuous and transient
224 overexpression, we found that the latter led to a much milder asymmetry than the former (Fig. 6C).
225 The transient expression experiment thus suggests that there is a catch-up mechanism that allows
226 limb growth to recover, and that would not have been discovered by irreversible misexpression,
227 highlighting the utility of the new mouse lines.
228
229 **The *Tigre*^{Dragon} lines are effectively activated by (r)tTA and Cre, and not leaky.**
230 We then performed in-depth characterization of the described lines, to ensure they were tightly and
231 efficiently regulated in a variety of scenarios. In previous studies we showed that *TRE*-driven
232 transgenes are highly expressed from the *Tigre* locus when insulator elements and a Woodchuck
233 virus RNA stabilizing sequence are included (Madisen et al., 2015; Rosello-Diez et al., 2018).
234 However, it has not been tested whether the TRE in the *Tigre*^{Dragon} lines drive expression of GOIs at
235 a high level in the presence of other *TREs* that could compete for the transcriptional machinery and
236 rtTA. This is important because one possible non-intersectional application of our system is to
237 combine it with an (r)tTA and a TRE-driven Cre to achieve expression of both Cre and the GOI in a
238 tissue during the time (r)tTA is activated. To address potential competition between TRE-driven
239 transgenes, we generated mice bearing a *TRE-Cre* (Perl et al., 2002), our *Col2a1-tTA* allele–which
240 initiates expression in the cartilage at around E12.5 (Rosello-Diez et al., 2018)–and the *Tigre*$^{Dragon\text{-}p21}$
241 allele (*TC-Cart-p21* model, Fig. 7A,B). We analyzed the mice at postnatal day (P) 0 in the
242 absence of Dox, such that the tTA was active for at least a week before analysis. In *Tigre*$^{Dragon\text{-}p21}$

243 mice that lacked both *tTA* and *TRE-Cre*, no tdTom or p21 expression was detected in the target
244 tissue (or other tissues), confirming that there is no spontaneous expression of the *Dragon* allele
245 (Fig. 7C and C' left). In the presence of only *tTA*, ectopic expression of almost only tdTom was
246 found in the cartilage (Fig. 7C middle), and the intensity of the few $p21^{+}$ cells was barely above
247 background (Fig. 7C' middle, D), revealing there is negligible read-through activity past the STOP
248 cassette. Finally, when both *TRE-Cre* and *tTA* were present along with the $Tigre^{Dragon\text{-}p21}$ allele, we
249 observed only p21 expression, demonstrating a full switch from $Tigre^{TRE}$-driven tdTom to p21
250 expression (Fig. 7C, C', D). Since no cells expressed only tdTom in this genetic combination, this
251 result indicates that the two *TRE*-driven alleles are both effectively induced.
252
253 **A germline-recombined version of the $Tigre^{Dragon}$ allele is controlled by (r)tTA only.**
254 In cases where intersectionality is not a priority, to avoid the extra breeding steps required to
255 introduce a third allele such as *TRE-Cre*, we have also generated a germline-recombined version of
256 the $Tigre^{Dragon\text{-}p21}$ allele ($Tigre^{TRE\text{-}p21}$ or *p21rec,* Fig. 8A) that only requires (r)tTA activity to
257 express *p21*. To characterize this allele, we generated mice containing *Col2a1-rtTA, p21rec* and
258 *Pitx2-Cre* (the latter for control purposes, *Cart-p21* model). As expected, when we provided Dox to
259 induce rtTA activity at E12.5, since p21 expression does not require intersection with Cre activity,
260 there was no significant left-right difference in the number of chondrocytes expressing p21 (Fig.
261 8B,C). Moreover, a higher percentage of chondrocytes expressed p21 in the limbs (~80%, Fig.
262 8B,C) than in the left limb of the intersectional approach (50-60% in Dox-treated *Pitx2-Cre/+;*
263 *Col2a1-rtTA;* $Tigre^{Dragon\text{-}p21}$ mice, (Rosello-Diez et al., 2018)). This new *p21rec* strain and similar
264 derivatives that could be generated from our *DTA* and *Ctgf Dragon* alleles will be useful to interfere
265 with cell functions in a variety of contexts, either by using existing tissue-specific (r)tTA mouse
266 lines or Cre-dependent (r)tTAs activated by tissue-specific Cre.
267
268 **The *Dragon* targeting vectors can be used for *in ovo* electroporation.**
269 Lastly, we tested the possibility of using the $Tigre^{Dragon}$ tools in animal models other than the
270 mouse. The chicken embryo has been a classical model for cell and developmental biology,
271 immunology, virology and cancer that is experiencing a revival since the introduction of modern
272 genetic and imaging tools (Kain et al., 2014; Rashidi and Sottile, 2009; Stern, 2005). *In ovo*
273 electroporation enables the introduction of exogenous genetic constructs in multiple locations of the
274 embryo, in order to perform gain- and loss-of-function studies, lineage tracing, live imaging, etc.
275 (Morin et al., 2017; Scaal et al., 2004). Therefore, we electroporated the right half of the neural tube
276 of chicken embryos at Hamilton-Hamburger (HH) stage 14-17 (Hamburger and Hamilton, 1992)
277 with a mix of *pCAGGS-H2B-TagBFP* (to visualize electroporated cells), *pCAGGS-rtTA-IRES-Cre*

278 (to constitutively express rtTA and Cre) and a *Tigre* targeting vector (*Ai62*) bearing a *TRE-*
279 *loxSTOPlox-tdTomato* cassette (Madisen et al., 2015). 16h after electroporation, Dox was provided
280 (1 µg per egg). 24 h after electroporation, we observed robust and consistent electroporation (blue
281 signal, Fig. 9A) in the right neural tube of most surviving embryos, as well as strong red signal in
282 the electroporated area of Dox-treated embryos (Fig. 9A, C, n=11). Embryos not treated with Dox
283 did not show any tdTom signal (Fig. 9B, n=3).
284 Lastly, we took advantage of chicken embryo accessibility to try an orthogonal approach. In this
285 case, only pCAGGS-rtTA and the *Tigre* construct were electroporated, while the Cre was added as
286 a fusion protein (TAT-Cre). The TAT peptide allows the Cre to cross membranes (Gitton et al.,
287 2009), such that when beads loaded with TAT-Cre are implanted near the electroporated area, the
288 Cre diffuses a few cell diameters away. The Cre then activates the GOI only in the electroporated
289 cells that are close to the bead, and only in response to Dox (Fig. 10A,B, n=6). Control embryos
290 electroporated with the full mix, but without bead (n=5, not shown), or implanted with PBS-soaked
291 beads (Fig. 10C, n=5), or electroporated with a mix devoid of rtTA and implanted with TAT-Cre
292 beads (Fig. 10D, n=5) did not show any $tdTom^{+}$ cells.
293
294 **DISCUSSION**
295 In this report, we have expanded and further tested the repertoire of $Tigre^{Dragon}$ intersectional tools
296 and demonstrate their advantages for in vivo studies. Given that there are currently over 3,000 Cre /
297 CreER lines (http://www.informatics.jax.org/downloads/reports/MGI_Recombinase_Full.html),
298 hundreds of which are available in repositories, and >200 (r)tTA lines (almost half of them in
299 repositories, see https://www.tetsystems.com/fileadmin/downloads/transgenic_mouse_lines/18-06-
300 07_table_1_ta.pdf), the potential combinations with the tools we describe here are extremely
301 numerous, allowing for very nuanced studies. As these numbers keep increasing, we anticipate that
302 the $Tigre^{Dragon}$ system will be useful to many developmental biologists and other life scientists
303 across different fields. The three main mouse lines described here ($Tigre^{Dragon\text{-}p21}$, $Tigre^{Dragon\text{-}DTA}$
304 and $Tigre^{Dragon\text{-}Ctgf}$) are being imported by the JAX repository (stocks # 034777-034779) to make
305 them available for the scientific community. It should be noted that these lines can be maintained in
306 homozygosity with no apparent phenotype, although after several generations of inbreeding some of
307 the homozygous animals show reduced fertility. Our labs mostly maintain these lines in an outbred
308 SwissWebster background. No parent-of-origin effects have been observed for these alleles. The
309 DNA constructs are in the process of being submitted to Addgene (#140894-140896).
310
311 $Tigre^{Dragon\text{-}DTA}$
312 We have shown, both in cerebella and limbs, that the $Tigre^{Dragon\text{-}DTA}$ line can be used for specific

313 ablation of particular cell populations, restricted to a temporal window of interest. Coupled to the
314 vast number of possible combinations of *Cre* and *(r)tTA* lines, the *Tigre*$^{Dragon\text{-}DTA}$ strain will be a
315 valuable resource to ablate cells at any developmental stage and location, allowing for systemic and
316 local responses to cell loss to be studied, including the activation of signaling pathways in response
317 to altered cell density and regenerative mechanisms to replenish cells that are lost.
318
319 *Tigre*$^{Dragon\text{-}Ctgf}$
320 CTGF is a pleiotropic molecule, which makes it difficult to elucidate its specific roles by traditional
321 overexpression approaches in which several locations and cell types are affected. Conversely, the
322 intersectionality of our approach enables targeting more precisely to a defined region, during a time
323 window of interest. This approach will enable the elucidation of tissue-specific roles of CTGF,
324 which should positively impact on regenerative medicine applications, tissue engineering and
325 developmental biology research.
326
327 *Avian experiments*
328 Our results indicate that the plasmids we have generated for mouse ES cell targeting can be directly
329 used for efficient *in ovo* electroporation, opening the door for precise gene manipulation in other
330 animal models. The use of tissue-specific rather than ubiquitous promoters would make the system
331 more versatile in the future. The orthogonal approach we describe using TAT-Cre enables a number
332 of experimental approaches with high spatial and temporal precision. For example, after
333 electroporation of the *rtTA* and the *Dragon* construct at an early stage, one can implant Cre-loaded
334 beads in a very localized region of the embryo when it is still accessible, and defer Dox
335 administration to a later time point such that the GOI can be activated even if the embryo has sunk
336 or turned in the egg.
337
338 *Comparison with existing systems*
339 Our system complements some of the existing sophisticated mouse genetic tools developed by the
340 community over the last few years. For example, Belteki et al. (Belteki et al., 2005) combined tissue
341 specific Cre with Cre-inducible rtTA and a TRE-controlled transgene to achieve conditional,
342 inducible and reversible transgene expression. That system however is not intersectional, since the
343 specificity depends only on the promoter driving Cre. Using the same number of transgenes (three)
344 our strategy achieves the additional feature of refined spatial control. A similar system reduced the
345 number of transgenes by making the rtTA and TRE-controllable cassettes part of a bicistronic
346 cassette (Haenebalcke et al., 2013). However, the cassette is targeted to the *Rosa26* locus, where the
347 TRE is prone to epigenetic inactivation (Godecke et al., 2017). Depending on the specifics of the

348 study being undertaken, our tools should allow approaches that were technically hindered before.
349 With regards to more recent tools involving CRISPR/Cas9 approaches, overexpression of
350 endogenous loci can be achieved via a nuclease-defective Cas9 fused to a transactivator domain in a
351 structure-optimized manner (Konermann et al., 2015). This strategy could be used to achieve results
352 similar to ours, if Cas9 were under the control of TRE with the sgRNAs in tandem, as recently
353 described (Jo et al., 2019). However, such a strategy would not be intersectional, nor would it allow
354 for misexpression of genes not present endogenously, such as DTA or genes harboring coding
355 mutations related to human disease. In summary, our approach fills a new niche in the ecosystem of
356 genetic tools, thus enabling new types of studies.
357
358 *Limitations and future directions*
359 One potential limitation of our vectors is that whereas the constructs work very well for transfection
360 *in vitro* using HEK cells (not shown) and for chicken embryo electroporation, they are probably not
361 suitable for efficient viral transduction, as they tend to be large (>10 kb) due to the inclusions of
362 insulators and RNA-stabilizing sequences.
363 Moreover, with the current system it is not possible to trace the lineage of the cells where the
364 intersectional activation took place, as the transgene stops being expressed when the (r)tTA is shut
365 down or the cells transition to another fate where (r)tTA expression is lost. Future versions could be
366 designed to express Flp recombinase in addition to the GOI, and combined with Flp-reporters to
367 indelibly label the lineage of the targeted population.
368
369 Lastly, we envision that the use of CreER instead Cre will introduce an additional level of control.
370 For example, the CreER could be used to prime a stem cell population shortly after an injury, such
371 that the descendants lose the loxSTOPlox cassette. In this scenario, only the descendants that
372 differentiate into an (r)tTA-expressing cell population of interest would be targeted, as opposed to
373 the whole set of descendants.
374
375 **MATERIALS AND METHODS**
376 *Reagents and resources*
377 See Supplementary Table 1.
378
379 *Generation and maintenance of mouse lines*
380 The generation of the *Tigre*$^{Dragon\text{-}p21}$ mouse line was as described (Rosello-Diez et al., 2018). To
381 generate the *Tigre*$^{TRE\text{-}p21}$ mouse line (aka *p21rec*), *Tigre*$^{Dragon\text{-}p21}$ males were crossed with germline
382 Cre-expressing females to delete the floxed cassette. The Cre allele was subsequently eliminated

383 during the breeding to generate *Tigre*$^{TRE\text{-}p21}$ homozygous animals.
384 To generate the *Tigre*$^{Dragon\text{-}Ctgf}$ mouse line, the *NruI*-STOP-loxP-tdTomato-*SnaBI* fragment in the
385 *Ai62(TITL-tdT) Flp-in* replacement vector (Madisen et al., 2015) was replaced by a custom *NruI-*
386 *tdTomato-STOP-loxP-MluI-HpaI-SnaBI* cassette, to generate an empty DRAGON vector. A PCR-
387 amplified Kozak-*Ctgf* cassette was subsequently cloned into the *MluI* and *SnaBI* sites to generate
388 the *DRAGON-Ctgf* vector. This vector was then used for recombinase-mediated cassette exchange
389 into *Igs7*-targeted G4 ES cells (Madisen et al., 2015). Two successfully targeted clones (#1 and #2)
390 were injected into C2J blastocysts to generate chimeras, obtaining 11 chimeric males that survived
391 (out of 30 animals born) with 25-85% chimaerism. One male from clone #1 and three males from
392 clone #2 were crossed to Swiss Webster mice (Charles River) to assess germline transmission. Only
393 clone #2 was successfully transmitted and used to establish the new mouse line.
394 A similar process was used to generate the *Tigre*$^{Dragon\text{-}DTA}$ mouse line, with the only difference
395 being that an attenuated version of DTA (tox176) was used to PCR-amplify the Kozak-DTA
396 cassette. Two successfully targeted clones (#8 and #13) were injected into C2J blastocysts to
397 generate chimeras, obtaining 34 chimeric males that survived (out of 52 animals born) with 35-
398 100% chimaerism. Four males from clone #8 and two from clone #13 were used to assess germline
399 transmission and establish the new mouse line.
400 All mouse lines were maintained on an outbred Swiss Webster background. *Atoh1-tTA, En1*^{Cre} and
401 *TetO-Cre* were genotyped as described (Kimmel et al., 2000; Perl et al., 2002) (Willett et al., 2019).
402 The DNA primers and programs used for genotyping the rest of alleles and transgenes are shown in
403 Supplementary Table 2.
404
405 *Animal experiments*
406 All mouse work was carried out according to institutional guidelines after obtaining their approval
407 (Sloan Kettering Institute IACUC and Monash University Animal Ethics Committee). For time-
408 mated crosses, vaginal plugs were checked in the mornings, and noon of the day the plug was
409 detected was considered E0.5. When Dox was needed, it was added to the drinking water. To
410 activate *Col2a1-rtTA*, the final concentration was 1 mg/ml, including 1% sucrose to increase
411 palatability. To inactivate *Col2a1-tTA* and *Atoh1-tTA*, the final concentration of Dox was 0.02
412 mg/ml.
413 Upon reception, chicken eggs were kept at 18ºC for up to 2 weeks. Two and half days prior to the
414 experiment, they were transferred to a watered incubator at 37ºC with forced ventilation.
415
416 *In ovo electroporation*
417 *In ovo* electroporation was performed as described (Blank et al., 2007). Briefly, on the day of the

418 experiment, eggs were laid out horizontally; 3 ml of albumin were removed from the blunt end of
419 each egg, and a window was opened on top with blunt forceps. A few drops of Ringer's solution
420 containing Penicillin-Streptomycin (Gibco 15140122, diluted 1/50) were pipetted on top, and the
421 membranes removed with a hooked needle. Indian ink (drawing ink A, Pelikan #201665, diluted
422 1/100 in Ringer's solution) was injected under the vitelline membranes to provide contrast. A pulled
423 glass capillary (Harvard apparatus GC120T-10) and a mouth pipette were used to inject into the
424 caudal neural tube the electroporation mix (1 µg/µl each plasmid in injection solution: high
425 viscosity carboxymethylcellulose 0.33% (Sigma); Fast Green 1% (Sigma); $MgCl_2$ 1 mM in PBS).
426 Custom-made electrodes (using 0.5-mm wide platinum wire for the positive electrode and a
427 tungsten wire for the negative one) were placed flanking the embryo, and a pulse generator (Intracel
428 TSS20 with current amplifier) used to deliver 3 square pulses (27 V, 30 ms ON, 100 ms OFF).
429 After electroporation, 200 µl of Doxycycline solution (5 ng/µl in Ringer's) were micropipetted
430 underneath the embryo. Eggs were then sealed with tape and incubated for 24h.
431 *Bead implantation*
432 Affigel blue beads were soaked at least 30 min in a solution of TAT-Cre (0.5 mg/ml in PBS), and
433 rinsed in PBS before grafting. Implantation was performed as described (https://bio-
434 protocol.org/e963), using a tungsten needle to open up a small section of the neural tube, and
435 forceps Dumont #5 to insert the bead inside the socket.
436
437 *Cloning of pCAGGS-rtTA-IRES-Cre*
438 The vector for constitutive expression of rtTA and Cre was built via Gibson cloning using Addgene
439 #20910 (digested *SmaI-PacI*) as backbone, and the following fragments: an *IRES* sequence
440 amplified from Addgene #102423 using primers
441 CTTGACATGCTCCCCGGGTAACCCCTCTCCCTCCCCCCC and
442 GCTCCATTCATTTATCATCGTGTTTTTCAAAGGAAAACCACG, and a Cre sequence
443 amplified from genomic DNA of a Cre^+ mouse with primers
444 AAACACGATGATAAATGTCCAATTTACTGACCG and
445 ATGCTCTCGTTAATCTAATCGCCATCTTCCAG. The molecular assembly was done with the
446 NEBuilder HiFi DNA Assembly cloning kit following manufacturer instructions.
447
448 *Sample collection and processing*
449 Mouse limbs: Upon embryo or pup collection, the limbs were dissected out in cold PBS, skinned
450 and fixed in 4% PFA for 2 days. No decalcification was done for samples P1 or younger. After PBS
451 washes, the limbs were cryoprotected in PBS with 15% sucrose and then equilibrated at 37ºC in
452 PBS with 15% sucrose and 7.5% porcine skin gelatin (Sigma) until they sank. The limbs were

453 oriented inside the wells of multi-welled plates and cooled down until solid, to then flash-freeze
454 them using a dry-ice cold bath of isopentane (Merck). The cryoblocks were sectioned at 7 µm on a
455 cryostat (Leica, CM3050S) onto Superfrost slides.

456 Mouse brains: The brains of all embryonic stages and P1 pups were dissected in cold PBS and
457 immersion fixed in 4% PFA for 24 hours at 4°C. P30 animals were transcardially perfused with PBS
458 followed by 4% PFA, and brains were post-fixed in 4% PFA overnight. Specimens for
459 cryosectioning were placed in 30% sucrose/PBS until they sank, embedded in OCT using
460 cryomoulds (Tissue-Tek), frozen in dry ice cooled isopentane, and sectioned at 14 µm on a cryostat
461 (Leica, CM3050S) onto Superfrost slides.

462 Chicken embryos: the embryos were scooped out of the egg and dissected in cold PBS. The
463 electroporated section of the trunk was isolated under the fluorescence scope and then fixed in 4%
464 PFA overnight. After PBS washes, specimens were cryoprotected in 15% sucrose and then 30%
465 sucrose in PBS, until they sank. They were then embedded in OCT using cryomoulds (Tissue-Tek),
466 frozen in dry-ice cooled isopentane, and sectioned at 7 µm on a cryostat (Leica, CM3050S) onto
467 Superfrost slides.
468
469 *Immunohistochemistry and TUNEL staining*

470 Mouse brains: Sections were incubator in PBS for 10 min and then blocked with blocking buffer
471 (5% Bovine Serum Albumin (BSA, Sigma) in PBS with 0.1% Triton X-100). Primary antibodies
472 (MEIS2, 1:3000) in blocking buffer were placed on slides overnight at 4°C, washed in PBS with
473 0.1% Triton X-100 (PBST) and applied with secondary antibodies (1:500 Alexa Fluor-conjugated
474 secondary antibodies in blocking buffer) for 1 hour at room temperature. Counterstaining was
475 performed using Hoechst 33258 (Invitrogen). The slides were then washed in PBST, then mounted
476 with a coverslip and Fluorogel mounting medium (Electron Microscopy Sciences). TUNEL staining
477 was performed prior to secondary antibody incubation using the Biotin-based in situ cell death
478 detection kit (Roche) and following the manufacturer instructions, including an Avidin-Biotin
479 blocking step (Vector Laboratories).
480
481 *In situ hybridization*
482 The DIG-labeled RNA probe for *Ctgf* was prepared by *in vitro* transcription of a PCR-amplified
483 template from embryonic day 12.5 cDNA, using the following primers: Fwd: 5'-
484 CAGCTGGGAGAACTGTGTAC-3', Rev(T7): 5'-
485 CGATGTTAATACGACTCACTATAGGGGCTCGCATCATAGTTGGGTC-3'.
486 Hybridization procedure as described in (Rosello-Diez et al., 2018).

487 *Skeletal preparations*

488 After embryo collection, the skin, internal organs and adipose tissue were removed. The samples
489 were then fixed in 95 % EtOH overnight at room temperature. To remove excess fat, the samples
490 were then incubated in acetone overnight at room temperature. To stain the cartilage, the samples
491 were submerged in a glass scintillation vial containing Alcian blue solution (0.04 % (w/v), 70 %
492 EtOH, 20 % acetic acid) and incubated at least overnight at room temperature. The samples were
493 destained by incubating them in 95 % EtOH overnight, and then equilibrated in 70% EtOH, prior to
494 being pre-cleared in 1 % KOH solution for 1-10h at room temperature (until blue skeletal elements
495 were seen through). The KOH solution was replaced with Alizarin red solution (0.005 % (w/v) in
496 water) for 3–4h at room temperature. The Alizarin red solution was then replaced with 1-2% KOH
497 until most soft tissues were cleared. For final clearing, the samples were progressively equilibrated
498 through 20% glycerol:80% (1%KOH), 50 % glycerol:50 % (1 %) KOH and finally transferred
499 to100 % glycerol for long-term storage.

500 *Image Analysis and Quantification*

501 The regions of interest were isolated from imaged sections of the multiple models. All the
502 parameters including the brightness, contrast, filters, layers were kept the same for all the images in
503 the same study. Cells positive for the signal of interest were counted manually using ImageJ, after
504 acquisition on an Imager Z1 microscope (Zeiss).
505

506 *Statistical Analysis*

507 The comparisons were done by an unpaired Mann-Whitney test (1 variable and 2 conditions), or by
508 2-way ANOVA (2 variables and 2 or more conditions) following a matched (paired) design when
509 possible (indicated when not). When left and right measurements were compared within
510 experimental animals only, Wilcoxon matched-pairs signed rank test was used. Non-parametric
511 tests were chosen when normality could not be confirmed. All the statistical analyses were done
512 using Prism7 software (Graphpad). No blinding was used except for Fig. 6C. Electroporated
513 chicken embryos were randomly assigned to control or experimental groups. No previous power
514 analysis was done to estimate the sample size.
515

516 **ACKNOWLEDGEMENTS**

517 We thank members of the Joyner and Rosello-Diez laboratories for discussions and technical help.
518 We are grateful to Dr. Miguel Torres for providing a polyclonal antibody to all isoforms of mouse
519 MEIS2, and to Megan Davey for sharing her expertise with TAT-Cre beads. We acknowledge the
520 assistance from Monash Animal Research Platform (MARP), Monash Micro Imaging Platform

(MMI) and the Sloan Kettering Institute Research Animal Resource Center and Mouse Genetics Core Facility. We also thank the Center for Comparative Medicine and Pathology and the Mouse Genetics Core Facilities of MSKCC for outstanding technical support. Plasmid *pT2-CAGGS-H2B-BFP* was a gift of the Marcelle lab. Addgene plasmids #20910 (*PB-CA-rtTA* Adv) and #102423 (*PB-CAGGS-rtTA-IRES-Hygro*) were donated by the Nagy and Koh labs, respectively.

COMPETING INTERESTS

There are no conflicts of interest.

FUNDING

This work was supported by grants from the Human Frontiers Science Program (LT000521/2012-L and CDA00021/2019) and Charles Revson Foundation (grant number 15-34) to A.R-D., Monash Graduate Scholarship (MGS), Monash International Tuition Scholarship (MITS) and the Islamic Development Bank (36/115444) funds to E.A., Postdoctoral fellowships to NSB (NYSTEM #C32599GG and NINDS K99 NS112605-01), NIH to A.L.J. (R21 HD083860, R37MH085726 and R01 NS092096) and a National Cancer Institute Cancer Center Support Grant (P30 CA008748-48). The Australian Regenerative Medicine Institute is supported by grants from the State Government of Victoria and the Australian Government.

AUTHOR CONTRIBUTIONS

E.A.: performed some *Tigre*$^{Dragon\text{-}Ctgf}$ and *Tigre*$^{Dragon\text{-}DTA}$ experiments and most chicken experiments and edited the manuscript; A.S.: performed data analysis and edited the manuscript; X.Q.: assisted with genotyping, cloning, embryo dissection, histology and data acquisition; N.S.B.: performed cerebellar experiments and analysis, D.S. assisted with breeding, genotyping and histology throughout the project; L.M. and H.Z.: performed ES cell targeting and provided key reagents; A.L.J was involved in experimental design, funding acquisition, supervision and manuscript editing; A.R-D. was responsible of conceptualization, funding acquisition, experimental design and procedures, data acquisition and analysis, supervision, manuscript drafting and editing.

REFERENCES

Belteki, G., Haigh, J., Kabacs, N., Haigh, K., Sison, K., Costantini, F., Whitsett, J., Quaggin, S. E. and Nagy, A. (2005). Conditional and inducible transgene expression in mice through the combinatorial use of Cre-mediated recombination and tetracycline induction. *Nucleic Acids Res* **33**, e51.

Blank, M. C., Chizhikov, V. and Millen, K. J. (2007). In ovo electroporations of HH stage 10 chicken embryos. *J Vis Exp*, 408.

557 **Breitman, M. L., Rombola, H., Maxwell, I. H., Klintworth, G. K. and Bernstein, A.** (1990).
558 Genetic ablation in transgenic mice with an attenuated diphtheria toxin A gene. *Mol Cell*
559 *Biol* **10**, 474-479.
560 **Brocard, J., Feil, R., Chambon, P. and Metzger, D.** (1998). A chimeric Cre recombinase
561 inducible by synthetic,but not by natural ligands of the glucocorticoid receptor. *Nucleic*
562 *Acids Res* **26**, 4086-4090.
563 **Dymecki, S. M. and Kim, J. C.** (2007). Molecular neuroanatomy's "Three Gs": a primer. *Neuron*
564 **54**, 17-34.
565 **Feil, R., Wagner, J., Metzger, D. and Chambon, P.** (1997). Regulation of Cre recombinase
566 activity by mutated estrogen receptor ligand-binding domains. *Biochem Biophys Res*
567 *Commun* **237**, 752-757.
568 **Feil, S., Valtcheva, N. and Feil, R.** (2009). Inducible Cre mice. *Methods Mol Biol* **530**, 343-363.
569 **Gitton, Y., Tibaldi, L., Dupont, E., Levi, G. and Joliot, A.** (2009). Efficient CPP-mediated Cre
570 protein delivery to developing and adult CNS tissues. *BMC Biotechnol* **9**, 40.
571 **Godecke, N., Zha, L., Spencer, S., Behme, S., Riemer, P., Rehli, M., Hauser, H. and Wirth, D.**
572 (2017). Controlled re-activation of epigenetically silenced Tet promoter-driven transgene
573 expression by targeted demethylation. *Nucleic Acids Res* **45**, e147.
574 **Gossen, M. and Bujard, H.** (1992). Tight control of gene expression in mammalian cells by
575 tetracycline-responsive promoters. *Proc Natl Acad Sci U S A* **89**, 5547-5551.
576 **Gossen, M., Freundlieb, S., Bender, G., Muller, G., Hillen, W. and Bujard, H.** (1995).
577 Transcriptional activation by tetracyclines in mammalian cells. *Science* **268**, 1766-1769.
578 **Haenebalcke, L., Goossens, S., Dierickx, P., Bartunkova, S., D'Hont, J., Haigh, K., Hochepied,**
579 **T., Wirth, D., Nagy, A. and Haigh, J. J.** (2013). The ROSA26-iPSC mouse: a conditional,
580 inducible, and exchangeable resource for studying cellular (De)differentiation. *Cell Rep* **3**,
581 335-341.
582 **Hamburger, V. and Hamilton, H. L.** (1992). A series of normal stages in the development of the
583 chick embryo. 1951. *Dev Dyn* **195**, 231-272.
584 **Hillen, W. and Berens, C.** (1994). Mechanisms underlying expression of Tn10 encoded
585 tetracycline resistance. *Annu Rev Microbiol* **48**, 345-369.
586 **Hirrlinger, J., Scheller, A., Hirrlinger, P. G., Kellert, B., Tang, W., Wehr, M. C., Goebbels, S.,**
587 **Reichenbach, A., Sprengel, R., Rossner, M. J., et al.** (2009). Split-cre complementation
588 indicates coincident activity of different genes in vivo. *PLoS One* **4**, e4286.
589 **Jo, N., Sogabe, Y., Yamada, Y., Ukai, T., Kagawa, H., Mitsunaga, K., Woltjen, K. and**
590 **Yamada, Y.** (2019). Platforms of in vivo genome editing with inducible Cas9 for advanced
591 cancer modeling. *Cancer Sci* **110**, 926-938.
592 **Kaczmarczyk, L. and Jackson, W. S.** (2015). Astonishing advances in mouse genetic tools for
593 biomedical research. *Swiss Med Wkly* **145**, w14186.
594 **Kain, K. H., Miller, J. W., Jones-Paris, C. R., Thomason, R. T., Lewis, J. D., Bader, D. M.,**
595 **Barnett, J. V. and Zijlstra, A.** (2014). The chick embryo as an expanding experimental
596 model for cancer and cardiovascular research. *Dev Dyn* **243**, 216-228.
597 **Kimmel, R. A., Turnbull, D. H., Blanquet, V., Wurst, W., Loomis, C. A. and Joyner, A. L.**
598 (2000). Two lineage boundaries coordinate vertebrate apical ectodermal ridge formation.
599 *Genes Dev* **14**, 1377-1389.
600 **Konermann, S., Brigham, M. D., Trevino, A. E., Joung, J., Abudayyeh, O. O., Barcena, C.,**
601 **Hsu, P. D., Habib, N., Gootenberg, J. S., Nishimasu, H., et al.** (2015). Genome-scale
602 transcriptional activation by an engineered CRISPR-Cas9 complex. *Nature* **517**, 583-588.
603 **Kronenberg, H. M.** (2003). Developmental regulation of the growth plate. *Nature* **423**, 332-336.
604 **Kubota, S. and Takigawa, M.** (2015). Cellular and molecular actions of CCN2/CTGF and its role
605 under physiological and pathological conditions. *Clin Sci (Lond)* **128**, 181-196.
606 **Machold, R. and Fishell, G.** (2005). Math1 is expressed in temporally discrete pools of cerebellar
607 rhombic-lip neural progenitors. *Neuron* **48**, 17-24.

608 **Madisen, L., Garner, A. R., Shimaoka, D., Chuong, A. S., Klapoetke, N. C., Li, L., van der**
609 **Bourg, A., Niino, Y., Egolf, L., Monetti, C., et al.** (2015). Transgenic Mice for
610 Intersectional Targeting of Neural Sensors and Effectors with High Specificity and
611 Performance. *Neuron* **85**, 942-958.
612 **Maes, C., Goossens, S., Bartunkova, S., Drogat, B., Coenegrachts, L., Stockmans, I.,**
613 **Moermans, K., Nyabi, O., Haigh, K., Naessens, M., et al.** (2010). Increased skeletal
614 VEGF enhances beta-catenin activity and results in excessively ossified bones. *EMBO J* **29**,
615 424-441.
616 **Matei, V., Pauley, S., Kaing, S., Rowitch, D., Beisel, K. W., Morris, K., Feng, F., Jones, K.,**
617 **Lee, J. and Fritzsch, B.** (2005). Smaller inner ear sensory epithelia in Neurog 1 null mice
618 are related to earlier hair cell cycle exit. *Dev Dyn* **234**, 633-650.
619 **Metzger, D., Clifford, J., Chiba, H. and Chambon, P.** (1995). Conditional site-specific
620 recombination in mammalian cells using a ligand-dependent chimeric Cre recombinase.
621 *Proc Natl Acad Sci U S A* **92**, 6991-6995.
622 **Morin, V., Veron, N. and Marcelle, C.** (2017). CRISPR/Cas9 in the Chicken Embryo. *Methods*
623 *Mol Biol* **1650**, 113-123.
624 **Perl, A. K., Wert, S. E., Nagy, A., Lobe, C. G. and Whitsett, J. A.** (2002). Early restriction of
625 peripheral and proximal cell lineages during formation of the lung. *Proc Natl Acad Sci U S*
626 *A* **99**, 10482-10487.
627 **Ponticos, M.** (2013). Connective tissue growth factor (CCN2) in blood vessels. *Vascul Pharmacol*
628 **58**, 189-193.
629 **Posey, K. L., Veerisetty, A. C., Liu, P., Wang, H. R., Poindexter, B. J., Bick, R., Alcorn, J. L.**
630 **and Hecht, J. T.** (2009). An inducible cartilage oligomeric matrix protein mouse model
631 recapitulates human pseudoachondroplasia phenotype. *Am J Pathol* **175**, 1555-1563.
632 **Rashidi, H. and Sottile, V.** (2009). The chick embryo: hatching a model for contemporary
633 biomedical research. *Bioessays* **31**, 459-465.
634 **Rosello-Diez, A., Madisen, L., Bastide, S., Zeng, H. and Joyner, A. L.** (2018). Cell-
635 nonautonomous local and systemic responses to cell arrest enable long-bone catch-up
636 growth in developing mice. *PLoS Biol* **16**, e2005086.
637 **Rosello-Diez, A., Stephen, D. and Joyner, A. L.** (2017). Altered paracrine signaling from the
638 injured knee joint impairs postnatal long bone growth. *Elife* **6**.
639 **Rosen, B., Schick, J. and Wurst, W.** (2015). Beyond knockouts: the International Knockout
640 Mouse Consortium delivers modular and evolving tools for investigating mammalian genes.
641 *Mamm Genome* **26**, 456-466.
642 **Scaal, M., Gros, J., Lesbros, C. and Marcelle, C.** (2004). In ovo electroporation of avian somites.
643 *Dev Dyn* **229**, 643-650.
644 **Sgaier, S. K., Lao, Z., Villanueva, M. P., Berenshteyn, F., Stephen, D., Turnbull, R. K. and**
645 **Joyner, A. L.** (2007). Genetic subdivision of the tectum and cerebellum into functionally
646 related regions based on differential sensitivity to engrailed proteins. *Development* **134**,
647 2325-2335.
648 **Shiratori, H., Yashiro, K., Shen, M. M. and Hamada, H.** (2006). Conserved regulation and role
649 of Pitx2 in situs-specific morphogenesis of visceral organs. *Development* **133**, 3015-3025.
650 **Smedley, D., Salimova, E. and Rosenthal, N.** (2011). Cre recombinase resources for conditional
651 mouse mutagenesis. *Methods* **53**, 411-416.
652 **St-Onge, L., Furth, P. A. and Gruss, P.** (1996). Temporal control of the Cre recombinase in
653 transgenic mice by a tetracycline responsive promoter. *Nucleic Acids Res* **24**, 3875-3877.
654 **Stern, C. D.** (2005). The chick; a great model system becomes even greater. *Dev Cell* **8**, 9-17.
655 **Takigawa, M.** (2013). CCN2: a master regulator of the genesis of bone and cartilage. *J Cell*
656 *Commun Signal* **7**, 191-201.
657 **Tarafder, S., Chen, E., Jun, Y., Kao, K., Sim, K. H., Back, J., Lee, F. Y. and Lee, C. H.** (2017).
658 Tendon stem/progenitor cells regulate inflammation in tendon healing via JNK and STAT3
659 signaling. *FASEB J* **31**, 3991-3998.

660 **Urlinger, S., Baron, U., Thellmann, M., Hasan, M. T., Bujard, H. and Hillen, W.** (2000).
661 Exploring the sequence space for tetracycline-dependent transcriptional activators: novel
662 mutations yield expanded range and sensitivity. *Proc Natl Acad Sci U S A* **97**, 7963-7968.
663 **Willett, R. T., Bayin, N. S., Lee, A. S., Krishnamurthy, A., Wojcinski, A., Lao, Z., Stephen, D.,**
664 **Rosello-Diez, A., Dauber-Decker, K. L., Orvis, G. D., et al.** (2019). Cerebellar nuclei
665 excitatory neurons regulate developmental scaling of presynaptic Purkinje cell number and
666 organ growth. *Elife* **8**.
667 **Zeng, H., Horie, K., Madisen, L., Pavlova, M. N., Gragerova, G., Rohde, A. D., Schimpf, B. A.,**
668 **Liang, Y., Ojala, E., Kramer, F., et al.** (2008). An inducible and reversible mouse genetic
669 rescue system. *PLoS Genet* **4**, e1000069.

670

671 **FIGURE LEGENDS**

672 **Figure 1. An intersectional genetic system for inducible and reversible gene misexpression.** A)
673 Basic components of the *Tigre*^{Dragon} alleles. Ins: insulators. W: Woodchuck virus RNA stabilizing
674 sequence (WPRE). Expression of the Gene of interest (GOI) depends on both Cre and (r)tTA. B-D)
675 In the presence of just (r)tTA (blue color in C and D), only the tdTomato (tdT) embedded in the
676 intact floxed cassette is expressed (top row in B, magenta color in C and D). In the presence of just
677 Cre (green color in C and D), the floxed tdTomato-STOP cassette is eliminated, priming the system
678 and deleting tdT, but the GOI is not expressed (middle row in B). It is only in the presence of both
679 Cre and (r)tTA (hatched blue and green in C and D) that the GOI is expressed (bottom row in B,
680 yellow color in C and D). As the expression of both tdT and the GOI depends on (r)tTA activity,
681 their expression is inducible and reversible, as it requires the presence of Doxycycline (Dox) for
682 rtTA to be active (C), or its absence in the case of tTA (D). E) Table summarizing the available
683 *Dragon* lines and their potential uses.
684

685 **Figure 2. A *Tigre*$^{Dragon\text{-}DTA}$ model to generate acute cell/tissue-specific cell ablation.** A, B)
686 Schematic showing *Tigre*$^{Dragon\text{-}DTA}$ allele and experimental plan. C-F) Sagittal sections through the
687 cerebellum of three types of E13.5 control embryos (*Tigre*$^{Dragon\text{-}DTA/+}$, *Atoh1-Cre/+; Tigre*$^{Dragon\text{-}DTA/+}$
688 and *Atoh1-tTA/+; Tigre*$^{Dragon\text{-}DTA/+}$) and an *AC-eCN-DTA* embryo in the absence of Dox. The boxed
689 areas are shown magnified in the lower panels. NTZ, nuclear transitory zone; VZ, ventricular zone;
690 RL, rhombic lip; EGL, external granule layer. Long arrows show the direction of the tangential
691 migration as the cells exit the RL. Arrowheads in the magnified boxes point to apoptotic cells
692 (TUNEL$^+$). (G). Quantification of cell death in the NTZ identified by MEIS2 staining on adjacent
693 sections (not shown) of E13.5 embryos as measured by the number of TUNEL$^+$ particles.
694 *Tigre*$^{Dragon\text{-}DTA/+}$ animals were used as controls (n=3/genotype, p=0.016, Mann-Whitney unpaired
695 test). (H, I) Sagittal sections through the cerebellum at P1, showing reduced numbers of MEIS2$^+$
696 eCN in *AC-eCN-DTA* mutants compared to a *Tigre*$^{Dragon\text{-}DTA/+}$ control. (J) Quantification of MEIS2$^+$
697 eCN number per half P1 cerebellum (every other section). *Tigre*$^{Dragon\text{-}DTA}$/+ animals were used as
698 controls (n=4/genotype, p=0.029, Mann-Whitney unpaired test). Scale bars = 100 μm.
699

700 **Figure 3. Intersectional capabilities of the *Tigre*$^{Dragon\text{-}DTA}$ model.** A) Schematic of *En1*-lineage
701 (based on (Sgaier et al., 2007)) and *Atoh1* expression (based on (Machold and Fishell, 2005)).
702 Striped regions represent hindbrain nuclei that are outside of the cerebellum. B-E) Representative
703 sagittal sections showing the cerebellar anlagen at E13.5 in control embryos (either *Tigre*$^{Dragon\text{-}DTA/+}$,
704 *En1*$^{Cre/+}$*; Tigre*$^{Dragon\text{-}DTA/+}$, or *Atoh1-tTA/+; Tigre*$^{Dragon\text{-}DTA/+}$) and *EC-eCN-DTA* embryos, in the
705 absence of Dox. Asterisk points to the loss of tdTom$^+$ cells in the NTZ and the two hindbrain nuclei
706 targeted by the intersectional approach and the arrowhead points to the hindbrain nuclei that are not
707 affected. The boxed areas are shown magnified in the right panels, rotated counter-clockwise. Insets
708 show cell death (TUNEL$^+$) in the rhombic lip region (RL). Arrows show the direction of the
709 tangential migration as the cells exit the RL. The boxed areas are shown magnified in the right

710 panels and were rotated counter clockwise. F) Quantification of cell death in the RL of E13.5
711 embryos detected by TUNEL (n=3/genotype, p=0.001, Mann-Whitney unpaired test). G)
712 Quantification of large NeuN$^+$ cells from every other sagittal section from half P30 cerebella shows
713 the number of excitatory cerebellar nuclei in *EC-eCN-DTA* animals as compared to controls (n=3
714 for both genotypes, p=0.029, Mann-Whitney unpaired test). H-I) Representative images of the P30
715 cerebella of *EC-eCN-DTA* (I) and littermate control (H). J) Quantification of cerebellar area of
716 midline sections shows reduction in cerebellar area after eCN ablation. Scale bars = 100 µm.
717 *Tigre*$^{Dragon\text{-}DTA/+}$ or *Atoh1-tTA/+; Tigre*$^{Dragon\text{-}DTA/+}$ animals were used as controls for the
718 quantifications shown in F, G and J. NTZ, nuclear transitory zone; VZ, ventricular zone; V,
719 ventricle; RL, rhombic lip; EGL, external granule layer.
720

721 **Figure 4. *Tigre*$^{Dragon\text{-}DTA}$ allows generation of structural damage and reduced local cell density**
722 **due to cell death in tissues with low cell motility such as cartilage.** A) Schematic of the unilateral
723 cartilage-specific cell ablation model. *Col2a1-tTA* (Tet-Off) starts to be expressed in the limbs at
724 ~E12.5, the same stage at which Dox was provided in the Tet-On model to activate *Col2a1*-driven
725 rtTA (and maintained until collection). B) TUNEL staining on E15.5 proximal humerus sections
726 shows increased apoptosis in the left cartilage as compared to the right. C) One week of continuous
727 DTA expression leads to the generation of acellular gaps in the left cartilage (dashed lines and
728 arrows). D) Quantification of TUNEL$^+$ cells in cartilage at P1 (n=4 *PC-DTA* and 5 *PC-Cart-DTA*).
729 2-way ANOVA results are shown. The bottom table shows the p-values for the different variables.
730 p-values within the graph are for Sidak's multiple comparisons test. E) Cell death in the cartilage
731 leads to impaired left-bone growth as compared to the contralateral one at P1 (representative femora
732 shown in top panel). Bone length ratios were analyzed by a mixed effects model (pGenotype
733 <0.0001), as some samples lacked matching femur-humerus measurements. p-values for Sidak's
734 multiple comparisons post-hoc test are shown on top.
735

736 **Figure 5. Unilateral overexpression of connective tissue growth factor leads to bone**
737 **asymmetry.** A) *PC-Cart-Ctgf* model to achieve misexpression of *Ctgf* in the cartilage of the left
738 limb. Note that *Col2a1-tTA* (Tet-Off system) is used in this model, such that tTA is active without
739 Dox (starting at ~E12.5). B, C) *In situ* hybridization for *Ctgf* mRNA in the distal radius cartilage
740 from WT (B) and *PC-Cart-Ctgf* mice (C) at P0-P1 (n=3). D) Representative examples of skeletal
741 preparations of left and right *PC-Cart-Ctgf* bones at the indicated stages (n=7 at E15.5, 6 at E17.5,
742 4 at P1, 5 at P5-P7).
743

744 **Figure 6. Different outcomes of transient vs. continuous expression of *Ctgf* in the cartilage of**
745 **the growing bones.** A) Schematics of the transient injury experiment. B) RNA in situ analysis of
746 expression of *Ctgf* in the proximal cartilage of left and right tibia of *PC-Cart-Ctgf* P0 pups, 2 days
747 after Dox administration at E17.5 (n=3). C) When transgenic *Ctgf* expression was shut down by
748 Dox treatment in the *PC-Cart-Ctgf* model (Dox at E17.5, analysis at P0-P1), the asymmetry was not
749 as extreme as in the case of continuous *Ctgf* misexpression (no-Dox condition). In the graphs,
750 quantification of left/right ratio of bone length is shown for control (tTA$^-$) and experimental
751 animals (tTA$^+$), treated or not with Dox. Analysis by 2-way ANOVA for Genotype and Treatment,
752 p-values for Sidak's multiple comparisons post-hoc test are shown. Since we used an internal ratio
753 (left/right length), data from femora and humeri were pooled together. They were treated as
754 independent samples because *Pitx2-Cre* has been shown to recombine with different efficiencies in
755 forelimb and hindlimb (Rosello-Diez et al., 2018).
756

757 **Figure 7. The *Dragon* lines are effectively activated by tTA and Cre, and not leaky.** A)
758 Depiction of the alleles that compose a *TC-Cart-p21* model (see text for details). B) Prediction of
759 expression domains [color code as in (A)] in the presence of *Col2a1-tTA* but absence of the Cre

760 allele (left), and when both Cre and tTA alleles are present along with *Dragon-p21* (right). R, L:
761 right and left limbs, respectively. C) Representative micrographs of immunohistochemistry for the
762 indicated proteins on proximal tibia sections from newborn littermates of the indicated genotypes
763 (*Tigre*$^{Dragon\text{-}p21}$ is common to all three). Dashed lines delimit the cartilage. Asterisks indicate
764 endogenous expression of p21 in muscle and perichondrium. No Dox was provided for these
765 experiments. C') 1.8X magnification of boxed areas in C). Only p21 staining is shown. D)
766 Quantification of p21 expression in control and experimental mouse sections (n=4 each). p-value
767 for unpaired Mann-Whitney test is shown.
768

769 **Figure 8. A germline-recombined version of the *Tigre*$^{Dragon\text{-}p21}$ allele becomes responsive to**
770 **active (r)tTA only.** A) Depiction of the recombined allele (*p21rec*) and how it works in the
771 presence of *Col2-rtTA* (*Cart-p21* model). Note that the crosses include *Pitx2-Cre* for control
772 purposes, even though it is not necessary for p21 expression. B) Representative micrograph
773 showing p21 expression in left and right proximal tibial cartilage at E16.5, 4 days after Dox
774 administration. C) Quantification and statistical analysis of p21^{+} cells in the proliferative zone (PZ,
775 delimited by dashed lines). p-value for Wilcoxon matched-pairs signed rank test is shown.
776

777 **Figure 9. The *Dragon* vectors can be used for *in ovo* electroporation.** A) Schematics of the
778 electroporation procedure in the neural tube of chicken embryos (cartoon), and representative
779 examples of the outcome (micrographs taken on a fluorescence dissecting microscope). B-C)
780 Individual and merged channels of transverse neural tube sections (dashed lines) from
781 electroporated chicken embryos, either untreated (B, n=3), or Dox-treated (C, n=11), 24 h after
782 electroporation. In order to be able to visualize the native fluorescence of BFP, we used a green
783 nuclear stain (SYTOX Green).
784

785 **Figure 10. Orthogonal *Dragon*-driven gene misexpression combining electroporation and**
786 **implantation of Cre-soaked beads.** A) Schematics of the procedure of electroporation followed by
787 bead implantation. B) Implantation of TAT-Cre beads (3 mg/ml) activates tdT expression in some
788 of the electroporated cells (TagBFP^{+}) close by, but not in cells farther than ~100 microns from the
789 bead. Native expression of TagBFP is shown. C, D) Control experiments with PBS-only beads and
790 a full electroporation mix (C, n=5) and Cre-beads in the presence of an electroporation mix lacking
791 the rtTA plasmid (D, n=5).
792

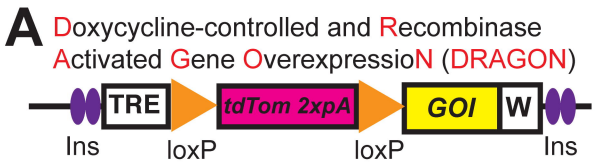

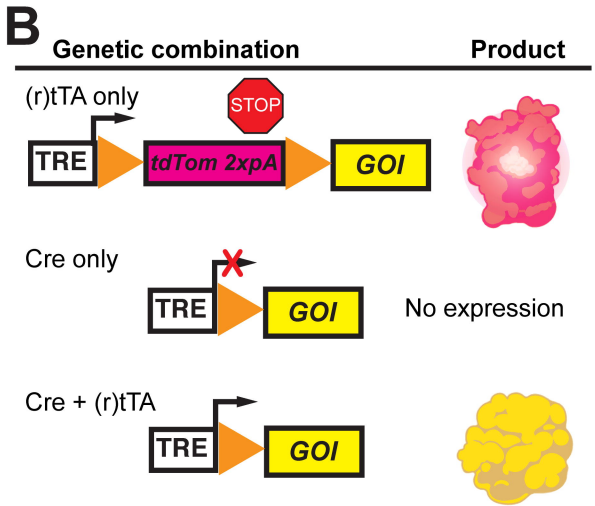

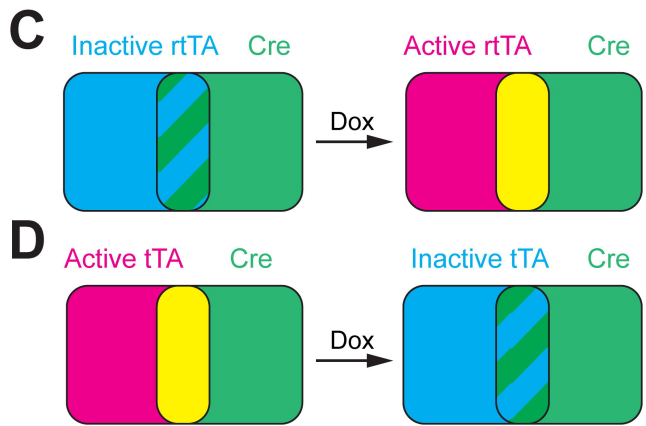

E

Available DRAGON mouse lines

GOI	Use	Described in
Cdkn1a (p21)	Block proliferation	Rosello-Diez et al. 2018
Ctgf (Ccn2)	Signal imbalance	This manuscript
DTA (Diphtheria toxin)	Cell ablation	This manuscript

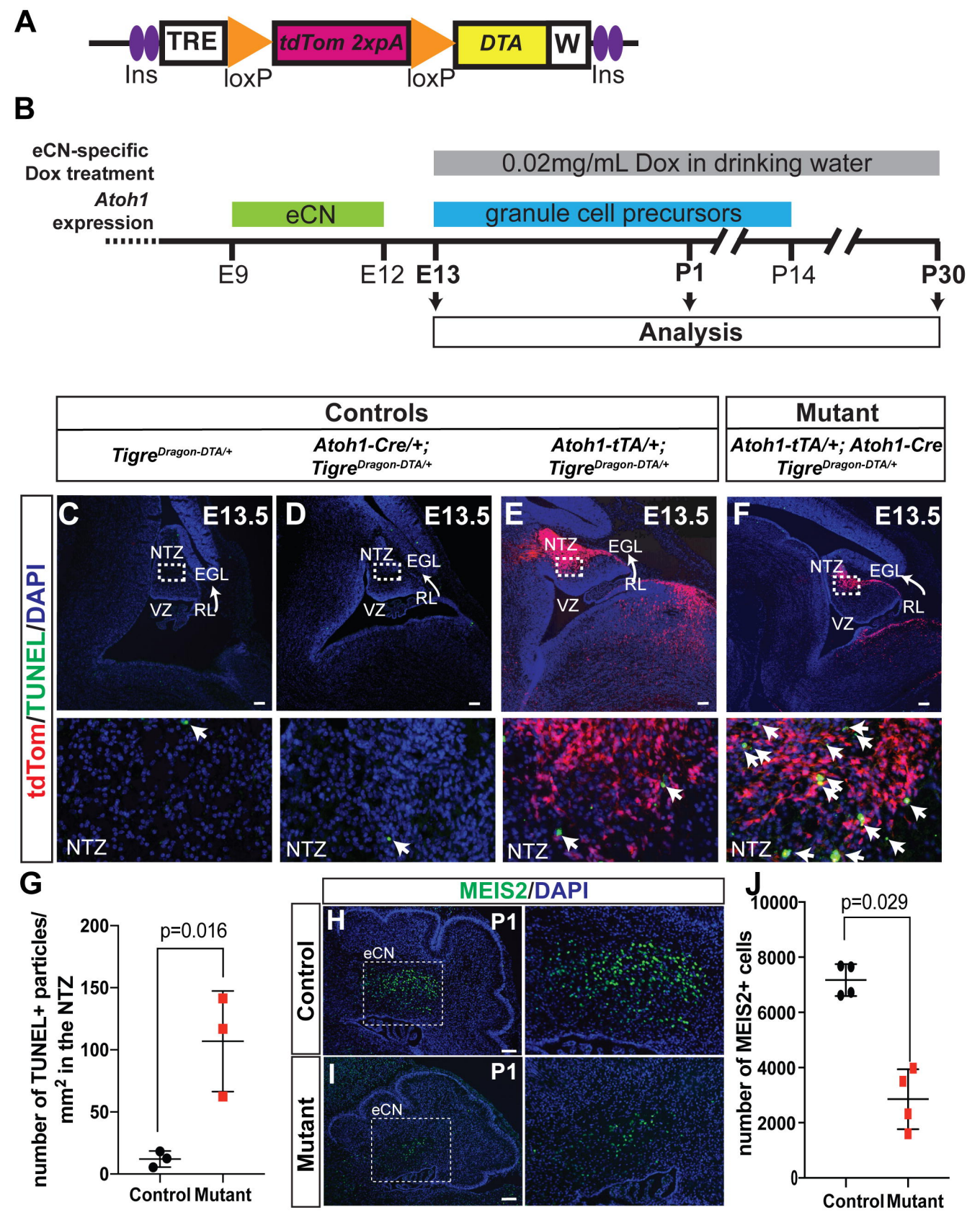
A
TRE
tdTom 2xpA
DTA
W
Ins
loxP
loxP
Ins
B
eCN-specific Dox treatment
0.02mg/mL Dox in drinking water
Atoh1 expression
eCN
granule cell precursors
E9
E12
E13
P1
P14
P30
Analysis
Controls
Mutant
Tigre Dragon-DTA/+
Atoh1-Cre/+; Tigre Dragon-DTA/+
Atoh1-tTA/+; Tigre Dragon-DTA/+
Atoh1-tTA/+; Atoh1-Cre Tigre Dragon-DTA/+
tdTom/TUNEL/DAPI
C
D
E
F
E13.5
NTZ
EGL
VZ
RL
G
number of TUNEL+ particles/ mm2 in the NTZ
p=0.016
Control
Mutant
MEIS2/DAPI
H
I
P1
eCN
Control
Mutant
J
number of MEIS2+ cells
p=0.029
Control
Mutant

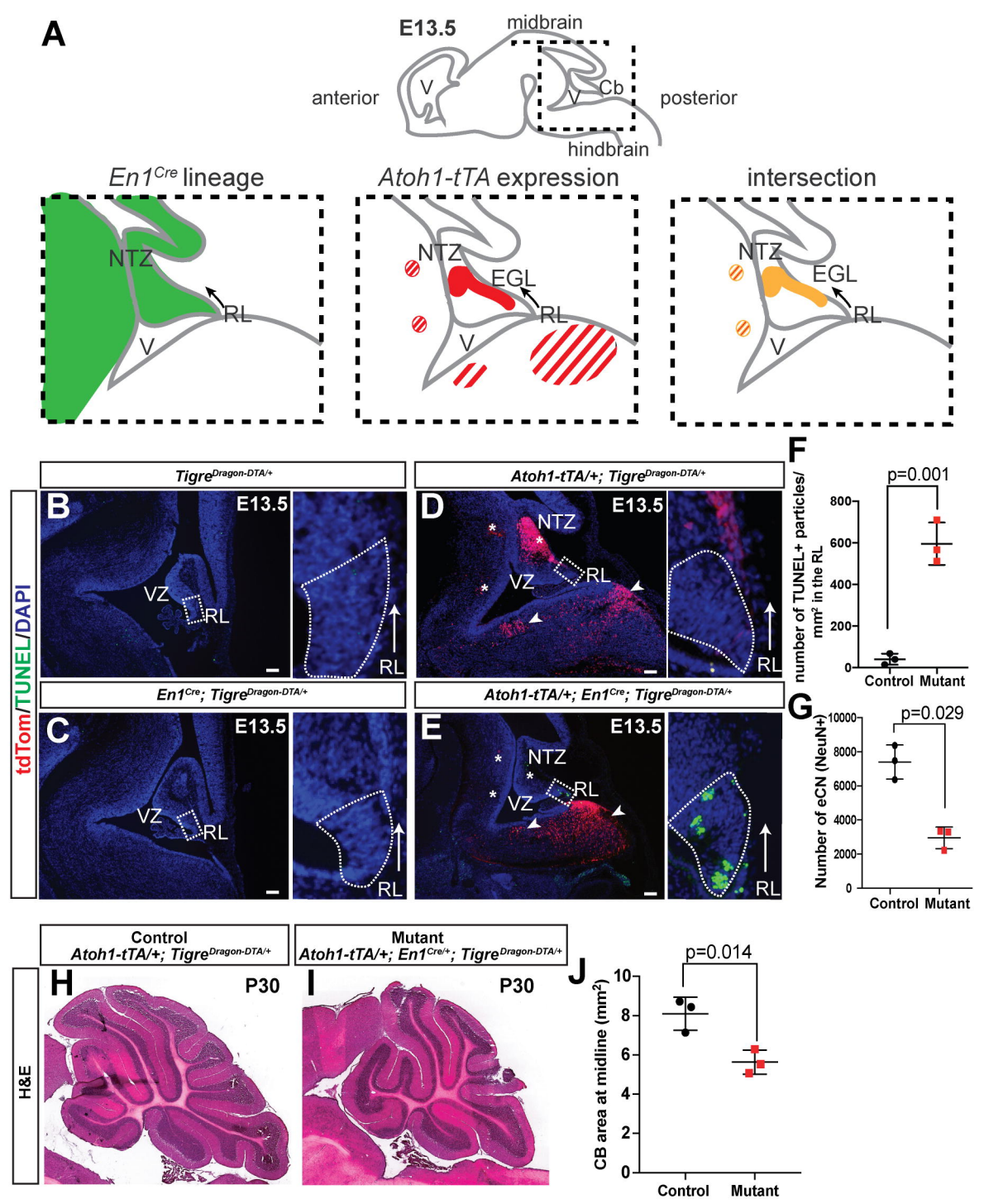
A
E13.5
midbrain
anterior
V
V
Cb
posterior
hindbrain
En1Cre lineage
Atoh1-tTA expression
intersection
NTZ
RL
V
NTZ
EGL
RL
V
NTZ
EGL
RL
V
Tigre Dragon-DTA/+
Atoh1-tTA/+; Tigre Dragon-DTA/+
En1Cre; Tigre Dragon-DTA/+
Atoh1-tTA/+; En1Cre; Tigre Dragon-DTA/+
tdTom/TUNEL/DAPI
B
C
D
E
E13.5
VZ
RL
NTZ
F
p=0.001
number of TUNEL+ particles/ mm2 in the RL
Control
Mutant
G
p=0.029
Number of eCN (NeuN+)
Control
Mutant
Control
Atoh1-tTA/+; Tigre Dragon-DTA/+
Mutant
Atoh1-tTA/+; En1Cre/+; Tigre Dragon-DTA/+
H&E
H
I
P30
J
p=0.014
CB area at midline (mm2)
Control
Mutant

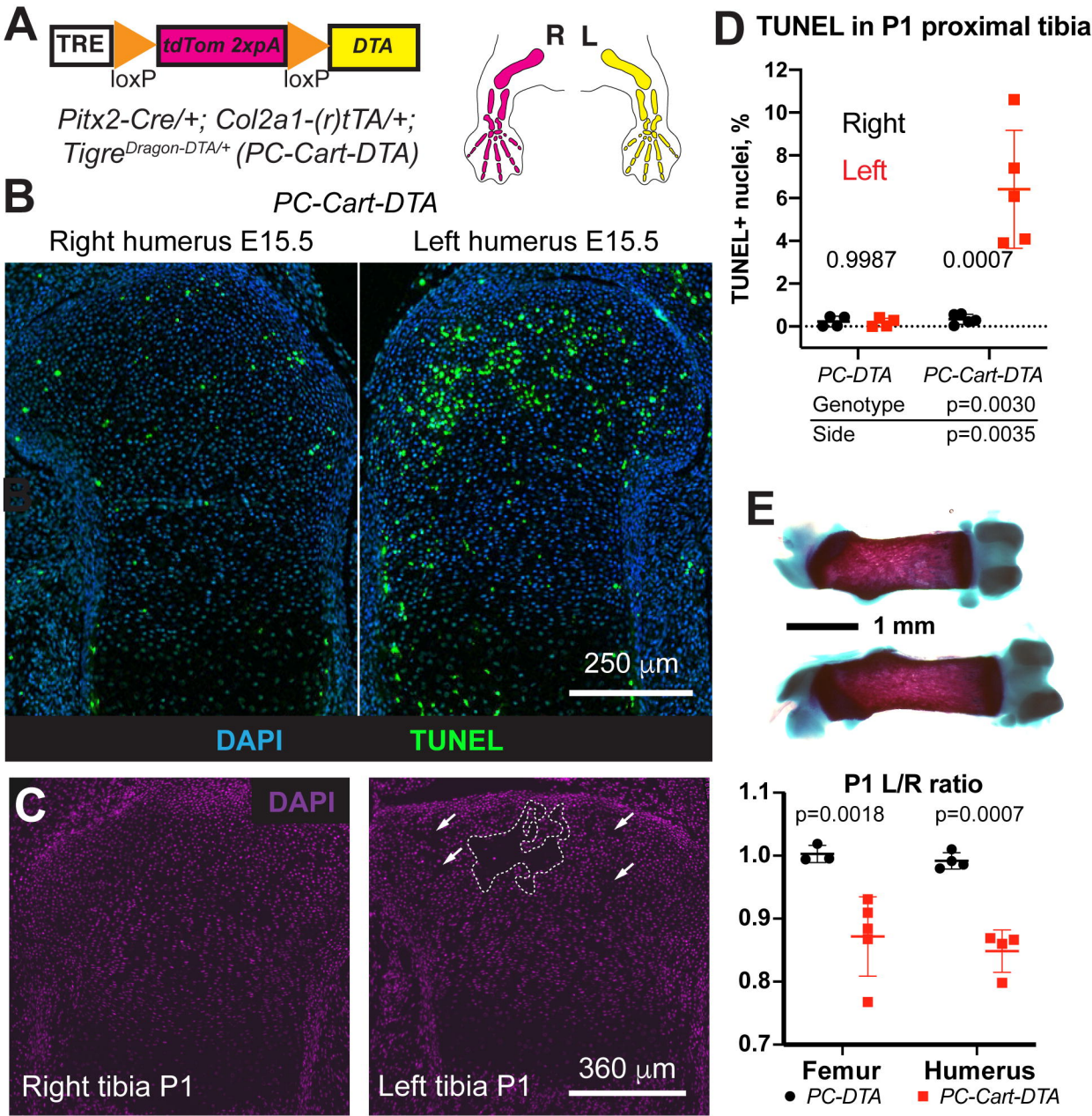
A
TRE
tdTom 2xpA
DTA
loxP
loxP
Pitx2-Cre/+; Col2a1-(r)tTA/+;
Tigre Dragon-DTA/+ (PC-Cart-DTA)
R L
B
PC-Cart-DTA
Right humerus E15.5
Left humerus E15.5
250 μm
DAPI
TUNEL
C
DAPI
Right tibia P1
Left tibia P1
360 μm
D
TUNEL in P1 proximal tibia
TUNEL+ nuclei, %
Right
Left
0.9987
0.0007
PC-DTA
PC-Cart-DTA
Genotype p=0.0030
Side p=0.0035
E
1 mm
P1 L/R ratio
p=0.0018
p=0.0007
Femur
Humerus
PC-DTA
PC-Cart-DTA

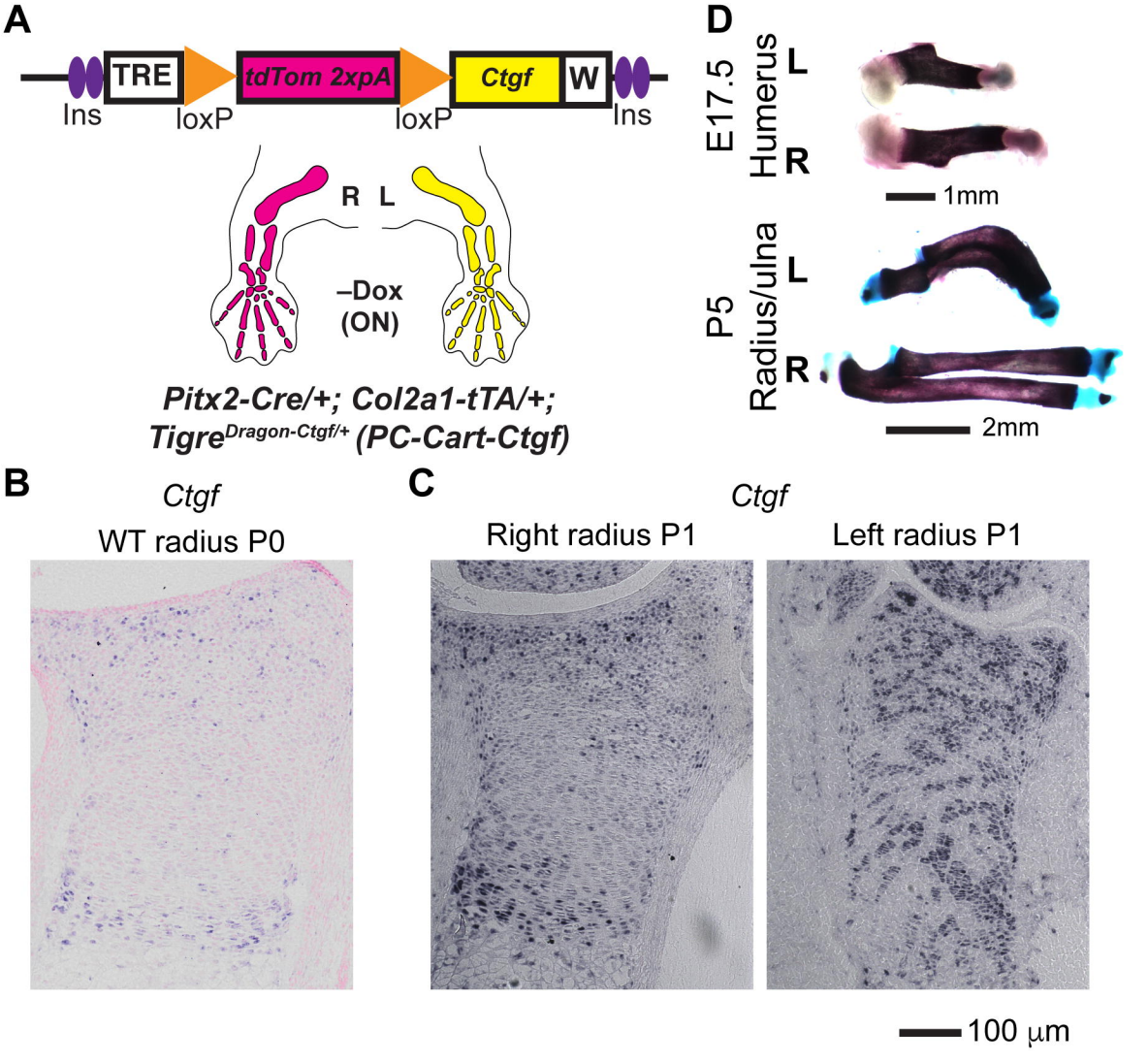
A
TRE
tdTom 2xpA
Ctgf
W
Ins
loxP
loxP
Ins
R L
–Dox
(ON)
Pitx2-Cre/+; Col2a1-tTA/+;
Tigre Dragon-Ctgf/+ (PC-Cart-Ctgf)
D
E17.5
Humerus
L
R
1mm
P5
Radius/ulna
L
R
2mm
B
Ctgf
WT radius P0
C
Ctgf
Right radius P1
Left radius P1
100 μm

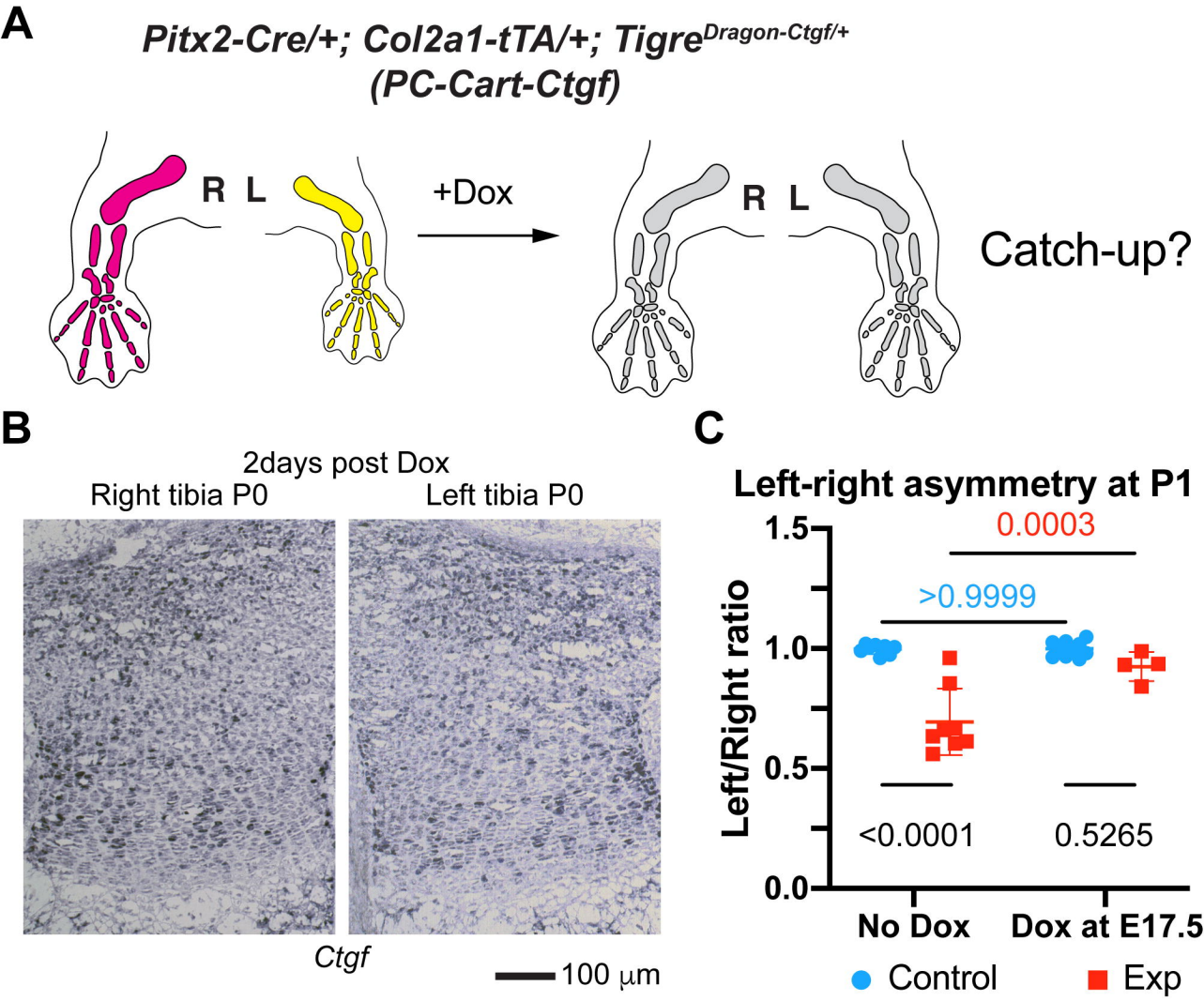
A
Pitx2-Cre/+; Col2a1-tTA/+; Tigre Dragon-Ctgf/+
(PC-Cart-Ctgf)
R L
+Dox
R L
Catch-up?
B
2days post Dox
Right tibia P0
Left tibia P0
Ctgf
100 μm
C
Left-right asymmetry at P1
Left/Right ratio
1.5
1.0
0.5
0.0
0.0003
>0.9999
<0.0001
0.5265
No Dox
Dox at E17.5
Control
Exp

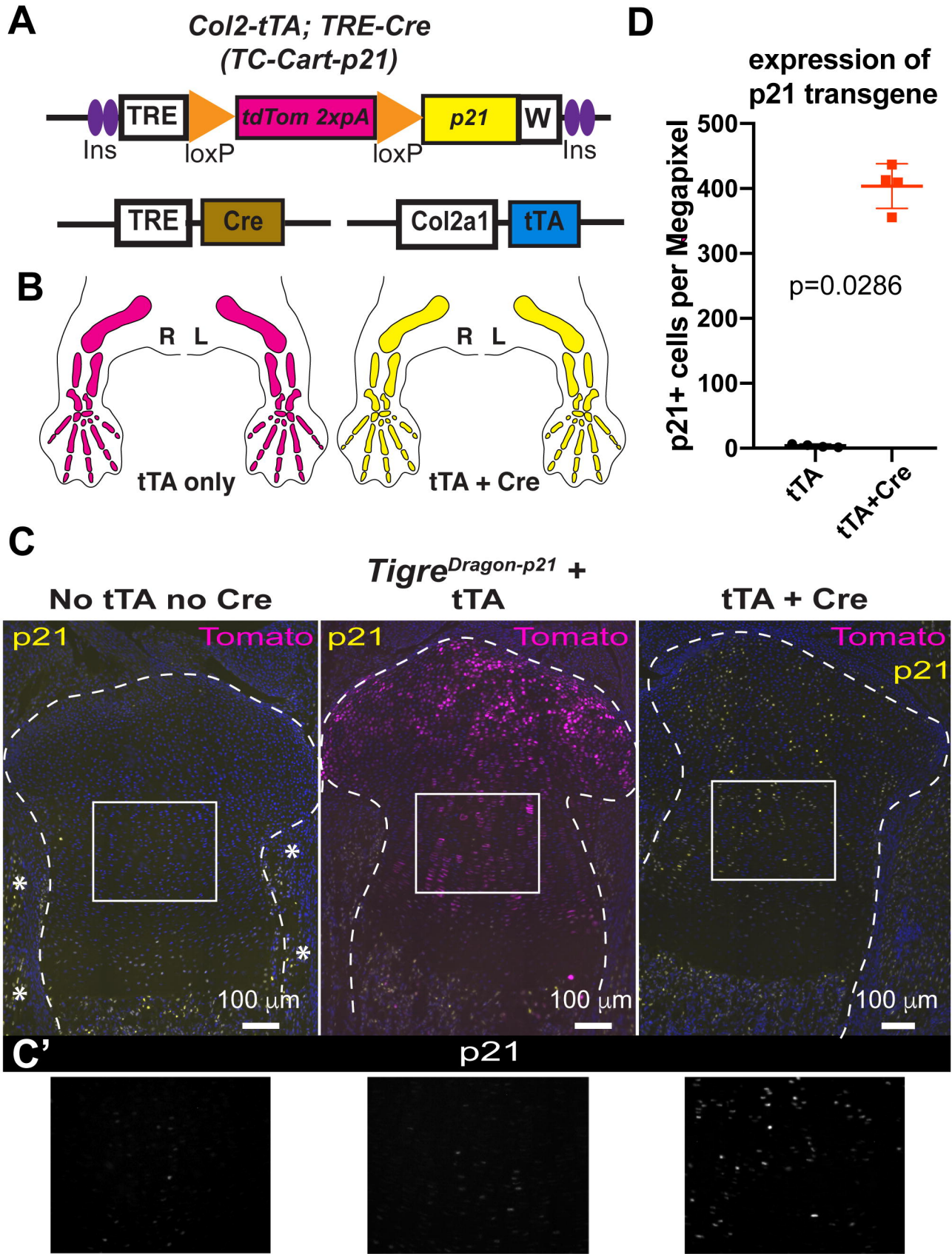
A
Col2-tTA; TRE-Cre
(TC-Cart-p21)
TRE
tdTom 2xpA
p21
W
Ins
loxP
loxP
Ins
TRE
Cre
Col2a1
tTA
B
R L
R L
tTA only
tTA + Cre
D
expression of
p21 transgene
p21+ cells per Megapixel
500
400
300
200
100
0
p=0.0286
tTA
tTA+Cre
C
Tigre Dragon-p21 +
No tTA no Cre
tTA
tTA + Cre
p21
Tomato
100 µm
C'
p21

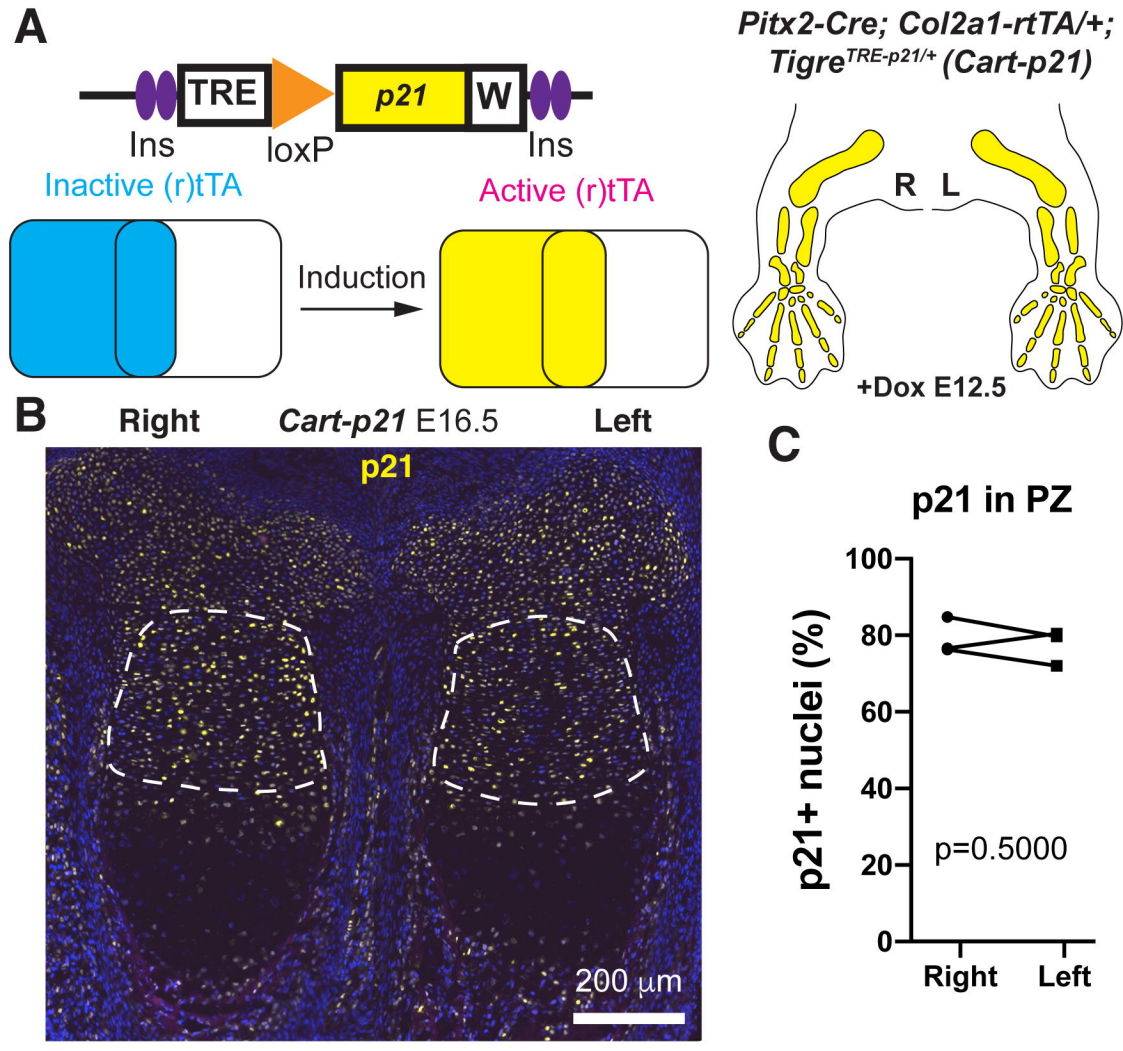
A
TRE
p21
W
Ins
loxP
Ins
Inactive (r)tTA
Active (r)tTA
Induction
Pitx2-Cre; Col2a1-rtTA/+;
Tigre TRE-p21/+ (Cart-p21)
R
L
+Dox E12.5
B
Right
Cart-p21 E16.5
Left
p21
200 μm
C
p21 in PZ
p21+ nuclei (%)
100
80
60
40
20
0
p=0.5000
Right
Left

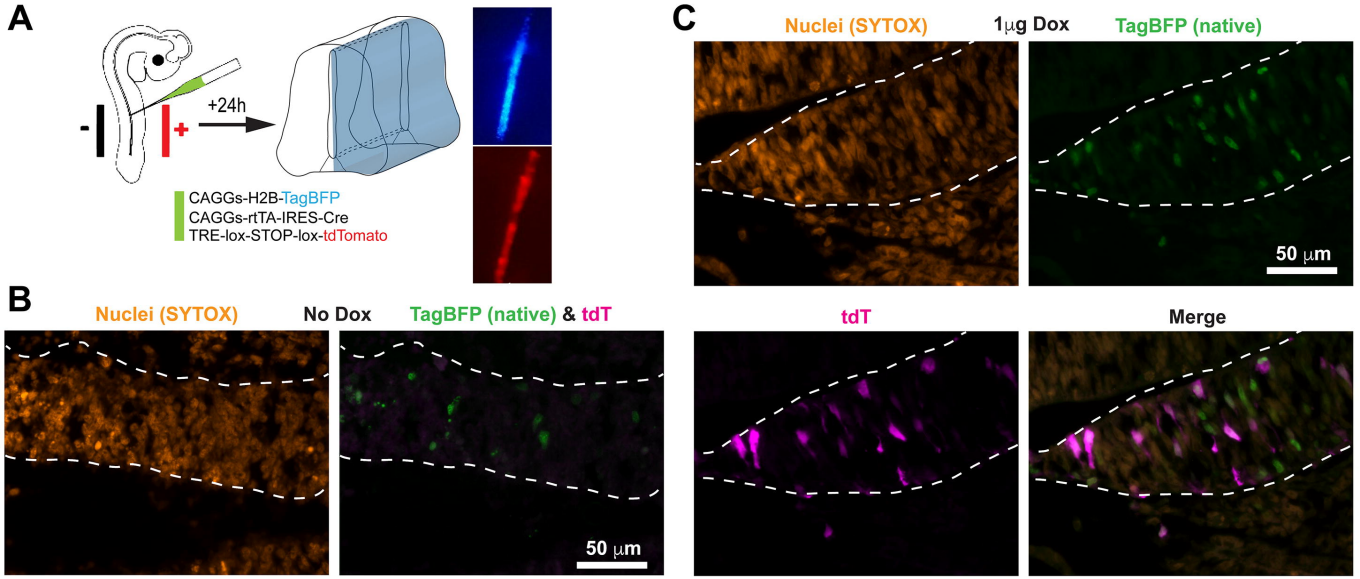
A
-
+
+24h
CAGGs-H2B-TagBFP
CAGGs-rtTA-IRES-Cre
TRE-lox-STOP-lox-tdTomato
B
Nuclei (SYTOX)
No Dox
TagBFP (native) & tdT
50 μm
C
Nuclei (SYTOX)
1μg Dox
TagBFP (native)
50 μm
tdT
Merge

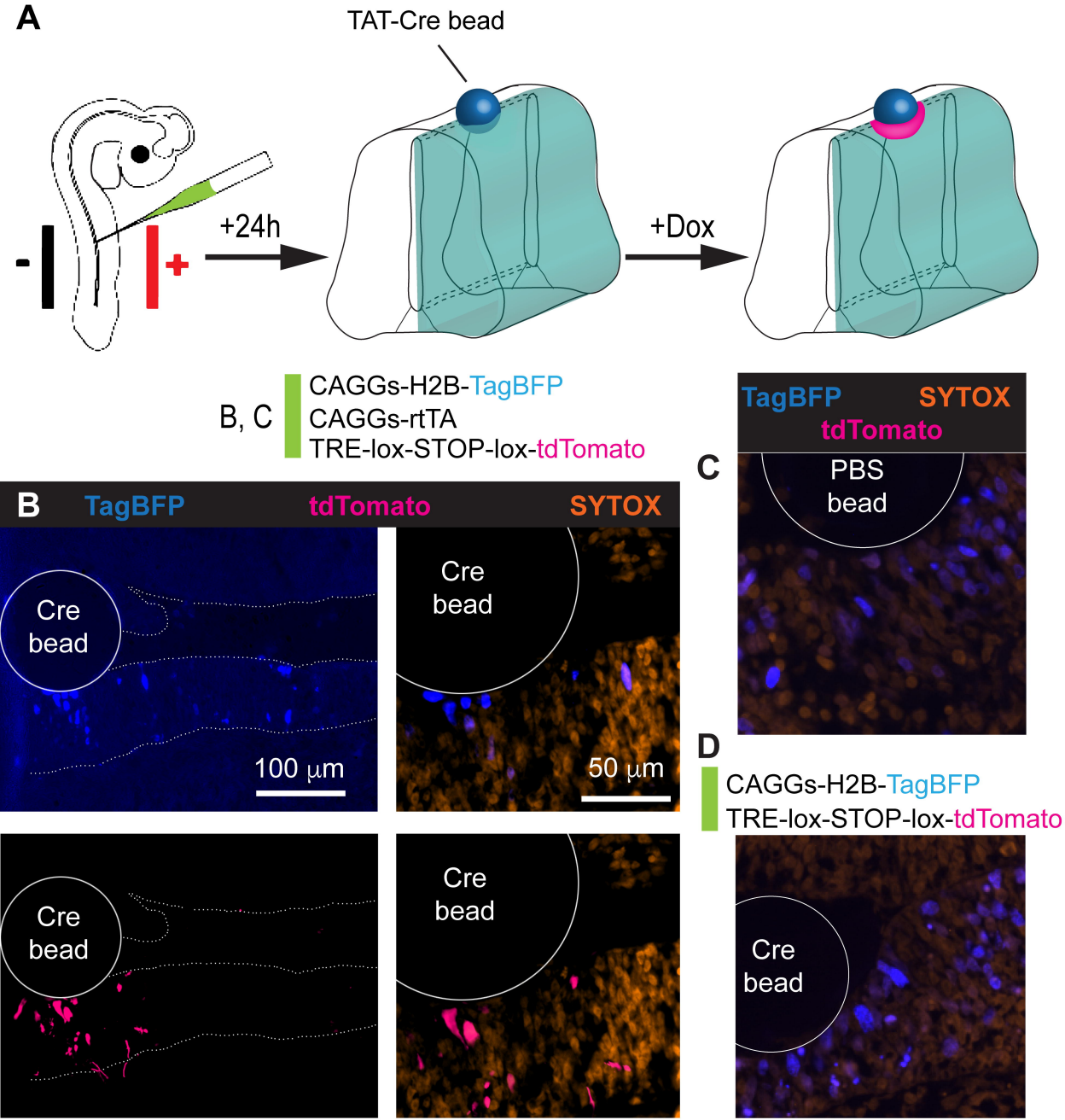
A
TAT-Cre bead
-
+
+24h
+Dox
B, C
CAGGs-H2B-TagBFP
CAGGs-rtTA
TRE-lox-STOP-lox-tdTomato
B
TagBFP
tdTomato
SYTOX
Cre bead
100 μm
Cre bead
50 μm
Cre bead
Cre bead
C
TagBFP
SYTOX
tdTomato
PBS bead
D
CAGGs-H2B-TagBFP
TRE-lox-STOP-lox-tdTomato
Cre bead